A neurometabolic signature in the frontal cortex explains individual differences in effort-based decision-making

Arthur Barakat[*,1], Nicolas Clairis[*,1], Jules Brochard[2], Mathias Pessiglione[3], Jean-Philippe Godin[4], Bernard Cuenoud[5,6] Lijing Xin[7,8], Carmen Sandi[1&]

[1]Laboratory of Behavioral Genetics (LGC), Brain Mind Institute (BMI), École Polytechnique Fédérale de Lausanne (EPFL), Lausanne, Switzerland

[2]Transdisciplinary Research Areas, Life and Health, University of Bonn, Bonn, Germany

[3]Motivation, Brain and Behavior team, Paris Brain Institute, Sorbonne University, Institut National de la Santé et de la Recherche Médicale, Centre National de la Recherche Scientifique, Paris, France

[4]Nestlé Research, Société des Produits Nestlé SA, Lausanne, Switzerland

[5]Nestlé Health Science, Epalinges, Switzerland

[6]Department of Medicine, Faculty of Medicine and Health Sciences, Université de Sherbrooke, Sherbrooke, Canada

[7]Center for Biomedical Imaging (CIBM), École Polytechnique Fédérale de Lausanne (EPFL), Lausanne, Switzerland

[8]Institute of Physics (IPHYS), École Polytechnique Fédérale de Lausanne (EPFL), Lausanne, Switzerland

* Equal contribution

[&] Corresponding & lead author: carmen.sandi@epfl.ch

Key words: Motivation; effort-based decision-making; mental effort; neurometabolism; ^{1}H-MRS; machine learning; dorsomedial prefrontal cortex; dorsal anterior cingulate cortex; anterior insula

Summary

Exploring why individuals vary in their willingness to exert effort is pivotal for understanding human motivation. Here, we utilized proton magnetic resonance spectroscopy (^{1}H-MRS) at 7 Tesla on the dorsomedial prefrontal cortex/dorsal anterior cingulate cortex (dmPFC/dACC) and anterior insula (AI) to uncover neurometabolic factors that influence these differences. Computational modeling and machine learning revealed that a model established on dmPFC/dACC metabolites explains decisions to exert high mental effort and sensitivity to mental effort but not physical effort. Glutamate, aspartate, and lactate in dmPFC/dACC were identified as key discriminative metabolites in the dmPFC/dACC, predictive of mental effort choices, whereas AI metabolism did not relate to effort-related decisions. Notably, there was a correlation between plasma and dmPFC/dACC lactate levels, suggesting a metabolic link between peripheral and central biomarkers of effort. Our findings provide novel insights into the neurometabolic underpinnings of motivated behavior and propose novel biomarkers for mental effort-based decision-making.

Introduction

Motivation drives individuals to overcome the inherent costs of actions to achieve desired outcomes, such as obtaining rewards or avoiding punishments [1,2]. This process, fundamental to human behavior, involves making decisions based on cost-benefit trade-offs between the rewards involved in an action and the effort required to reach them. However, there is striking variability in how individuals approach effortful decisions. Some readily engage in physically or mentally demanding tasks for potential gains or to avoid adverse outcomes, while others may show reluctance or inability to engage similarly, which can significantly impact their well-being, longevity, and success in life [3–5]. Moreover, a pronounced aversion to effort exertion is a key symptom in various brain pathologies [2,6]. While such diversity in motivational drive reflects a significant aspect of human cognition, our understanding of the neurobiological underpinnings of these inter-individual differences remains limited.

Neurobiologically, motivation and effort-based decision-making are closely linked to the functioning of specific brain regions, particularly the dorsomedial prefrontal cortex/dorsal anterior cingulate cortex (dmPFC/dACC) [2,7–10]. The dmPFC/dACC plays a pivotal role in driving mental and physical effort [11–13]. Lesions in this area can lead to increased effort aversion [14] and even akinetic mutism, a state characterized by a lack of initiative to act [15]. However, our understanding of the specific neurobiological components within the dmPFC/dACC that influence effort-based decision-making is still limited. Investigating these factors is vital for developing strategies to enhance motivation, thereby empowering individuals to achieve their goals and maximize their potential.

Recent advances emphasize the importance of brain bioenergetic and metabolic processes for brain function, behavior, and cognition [16–18]. While initial studies predominantly focused on glucose as a resource-limiting energy source for demanding cognitive processes [19,20], such as decision-making, evidence has revealed that brain glucose might not be a limited resource for brain processes as was originally proposed [21–24]. Moreover, neurons utilize various energy substrates, not just glucose, to support both neural structure and function [25–29] and, consequently, meet cognitive demands [18]. Importantly, several animal and human studies suggest that neurometabolic components in different brain regions are involved in decision-making and motivation [30–35]. These findings collectively reinforce the notion that cognitive processes, including motivation and decision-making, are closely linked to the brain's metabolic state. Understanding this relationship is crucial for insights into the mechanisms that regulate these cognitive functions. However, our understanding of how metabolism influences motivational processes and decision-making is still in its early stages.

Magnetic resonance spectroscopy (MRS) is emerging as a powerful non-invasive tool in this context, enabling the quantification of brain metabolites and providing insights into the neurochemical state

of specific brain regions. Proton (^{1}H)-MRS enables the quantification of several brain metabolites, such as glutamate, lactate, aspartate, N-acetylaspartate (NAA), creatine, and others. These metabolites play crucial roles in neuronal health, energy metabolism, and cellular signaling, all key for neural function and behavior production [36–38]. Understanding whether the concentrations of these metabolites in key brain regions are related to effort-based motivated processes can provide invaluable insights into the neurometabolic foundations of these cognitive functions. Previous human studies have offered initial evidence linking specific metabolites in specific brain regions to individuals' performance in motivation and decision-making tasks [32,34,39,40]. However, virtually all the studies linking metabolite concentrations, acquired through ^{1}H-MRS, to behavior or cognition have focused on individual metabolites using univariate analyses, whether in patient or healthy populations. This approach has led to a fragmented understanding, potentially overlooking how the combined influence of multiple metabolites contributes to motivated behavior. Addressing this gap by employing multivariate statistical methods can provide a more comprehensive view of the neurochemical bases of motivated behavior, given the interconnected nature of metabolic pathways.

In this study, we leveraged the critical role of the dmPFC/dACC in assessing cost-benefit trade-offs to explain individual differences in decision-making for effort-based motivated behavior. We utilized ultra-high field 7 Tesla (7T) ^{1}H-MRS to measure metabolite concentrations in the dmPFC/dACC and in the anterior insula (AI), as the AI that has also been involved in mental and physical effort [2,11,41], and both regions are key nodes of the brain salience network. Additionally, we conducted targeted metabolomic analyses of plasma samples. To gauge participants' willingness to exert physical and mental efforts, we created an effort-based decision-making task where subjects chose between a fixed low effort/low incentive option and a varying high effort/high incentive option. The task involved trials in which participants could obtain rewards or avoid punishment, alternating between mental and physical effort blocks. We applied computational modeling to extract key parameters influencing effortful decisions in our task, such as mental and physical effort perception [2,42]. We subsequently employed machine learning models to explore whether specific dmPFC/dACC and AI metabolite combinations could predict effortful choices and parameters of motivated behavior. Our study offers new insights into how the dmPFC/dACC -but not the AI- metabolic processes relate to motivated behavior components, potentially identifying novel biomarkers and therapeutic targets for motivation-related cognitive functions, especially in the context of mental effort and perception.

Results

Our study was designed to explore how individual variation in 7T ^{1}H-MRS measured metabolites in the dmPFC/dACC (see **Fig. 1a,c**) can predict differences in physical and mental motivated behavior (**Fig. 1d-e**) across individuals. Additionally, we performed ^{1}H-MRS scans in the AI to assess the specificity of our predictive findings (**Fig. 1b**). To minimize any external influences on the metabolic state of our participants, such as age, circadian rhythm, and meal effects, we implemented specific criteria. We included only individuals aged 25 to 40 years. Out of 75 participants recruited, data from 69 were fully valid for analyses (36 females; average age: 30 ± 4; BMI: 23.1 ± 3.2). We consistently started the experiments at 2 PM to minimize the potential effects of hunger, digestion, and circadian rhythms on our metabolic measurements.

Behavioral Task

To assess motivated behavior, participants performed a behavioral task comprising 216 trials in 4 blocks. To ensure task feasibility and prevent participants from perceiving decisions as risky, we calibrated the task individually during the training period (**Fig. 1**). In every trial, participants were presented with a choice between two options, characterized by differing monetary incentives and levels of required effort (**Fig. 1d-e**). These comprised a fixed low-effort option and a second option, where the effort level varied among three predefined levels. After making their choice, participants were required to perform the task at the selected effort level. This step was crucial to ensure that their decisions accurately reflected the presented effort levels. Notably, participants successfully completed the chosen effort in 95 ± 3.7% (mean ± SD) of the trials involving mental effort, and in 98 ± 3.4% of those requiring physical effort. Increased effort difficulty, associated with the high-effort option, resulted in fewer selections of high-effort/high-reward incentives in both physical and mental tasks **(Fig. S1a,d**), indicative of effort aversion. Additionally, higher difficulty levels not only demanded more effort but also led to tangible consequences: in the physical task, choosing the more effortful option correlated with increased and more intense handgrip force (**Fig. S1b-c**), while in the mental task, it resulted in a higher number of errors and elevated cognitive efficiency (**Fig. S1e-f**). These outcomes corroborate the task's effectiveness in quantifying motivational dynamics for both physical and mental efforts.

Importantly, the distribution of high mental effort choices and high physical effort choices, a proxy of motivated behavior (**Fig. S2**), was unaffected by sex differences, and were not correlated to one another ($r = 0.22$, $p = 0.06$).

dmPFC/dACC Metabolites Explain Motivated Behavior

To determine if dmPFC/dACC metabolite levels can predict the proportion of high mental effort (HME) and high physical effort (HPE) effort choices made by participants, we employed a gradient tree boosting regression model with metabolite concentrations as regressors. Our feature selection process, applied to 18 features including metabolites and standard ratios (detailed in Supplementary Materials), identified 9 features relevant for HME and 4 for HPE prediction (**Fig. 2**). To enhance data robustness and minimize overfitting, we adopted a train/validation/test approach with cross-validation leave-one-out (CVLOO) design, splitting data into training/validation and testing sets with an 80% ratio, resulting in training/validation (N = 55) and testing (N = 14) datasets. We trained extreme gradient boosting trees (XGBoost) to fit linear response functions to HME and HPE, utilizing Bayesian optimization for hyperparameter tuning. The prediction error of the model was quantified using the root mean square error (RMSE).

For HPE, the model showed a medium fit in training and validation (train RMSE = 0.16%, validation RMSE = 16.06%), and a non-significant result on the test set (test RMSE = 23.00%, r = 0.22, p = 0.22), explaining only 5% of the variance (**Fig. 2a**). A permutation test with 5000 permutations further indicated that these results were not above chance level (95th percentile = 13.38 > model RMSE = 23.00) (**Fig. 2b**), indicating that HPE could not be predicted with combinations of metabolites. Similarly, training a model on metabolites from the AI, resulted in poor, non-significant performance (test RMSE = 24.46%, r = 0.24, p = 0.4), leading us to discard HPE prediction from further analysis.

In contrast, for HME, the model developed demonstrated a good fit (train RMSE = 0.05%, validation RMSE = 13.06%) and a consistent result in the unbiased estimate that is the test set (test RMSE = 12.37%, r = 0.56, p = 0.036), explaining 31% of the variance (**Fig. 2c**). The permutation test with 5,000 permutations confirmed that our model's predictions significantly exceeded chance level (95th percentile = 13.72 > model RMSE = 12.37) (**Fig. 2d**). These results support our hypothesis that dmPFC/dACC metabolite concentrations can predict inter-individual variation in motivated behavior, specifically demonstrating their predictive power in the context of mental effort tasks.

To understand the impact of individual metabolites in the XGBoost model for predicting HME, we analyzed the Shapley Additive exPlanations (SHAP) values. The identified features included in descending order of their importance (determined by the magnitude of each feature's SHAP value) are glutamate (Glu), lactate (Lac), glutamine (Gln), taurine (Tau), N-acetylaspartate (NAA), N-acetylaspartylglutamate (NAAG), aspartate (Asp), glutathione (GSH) and creatine (Cr) (**Fig. 2e**). Thus, glutamate and lactate emerged as the top discriminating features. However, our SHAP analysis of the data distribution for each predictive feature/metabolite revealed that specific metabolite

concentrations do not always have a linear relationship with HME. Indeed, neither glutamate (r = -0.19, p = 0.12) nor lactate (r = -0.13, p = 0.27) demonstrated a linear relationship with HME. Particularly for glutamate, extreme values – either low or high – were negatively associated with HME, indicating a non-linear relationship. To further investigate this, we employed Bayesian model comparison to determine the best formula linking glutamate with HME. The model that most accurately predicted HME featured an inverted U-shape relation, based on the mean-centered squared score of glutamate concentrations (r = 0.36, p = 0.0026), as supported by both the Akaike Information Criterion (AIC) and Bayesian Information Criterion (BIC) (**Fig. S3**). However, no clear pattern could be observed when investigating lactate relationship with HME, supporting the view that its contribution lies in the multivariate model. In addition, the SHAP analysis also identified the importance of other metabolites, such as glutathione and taurine related to antioxidant pathways, and glutamine, to a lesser extent. Previous research showed a positive involvement of glutathione in the nucleus accumbens on the regulation of physical effort exertion [35], while glutamine levels in the nucleus accumbens were negatively related to physical effort perception [32]. These findings suggest that metabolic pathways impacting motivated behavior may vary across different brain areas.

To determine if the metabolites relevant for HME are specific to the dmPFC/dACC region, we similarly assessed the ability of AI metabolite concentrations to predict HME. We applied the same model training process used for the dmPFC/dACC to AI metabolite concentrations. However, this AI-based model did not achieve statistical significance in predicting HME in our test set (r = -0.47, p = 0.11) (**Fig. 2f**), nor in the permutation test (95th percentile = 13.89% > model RMSE = 23.28%) (**Fig. 2g**). These results underscore the specificity of the XGBoost model for the dmPFC/dACC in accurately predicting HME, thereby emphasizing the distinct predictive value of the dmPFC/dACC metabolic landscape in motivated behavior.

Dissecting Performance: Computational Modeling of Motivated Behavior

Thus far, our analysis has demonstrated the capability of dmPFC/dACC metabolites to predict HME using XGBoost. However, since motivation, and by extension HME, is a complex construct composed of multiple elements like reward sensitivity, effort aversion, etc. [1,2,42], the specific behavioral components related to metabolism in this brain region remain to be elucidated. We designed our task and a computational model in order to disentangle the different behavioral parameters that could influence HME in our task, namely different sensitivities to reward (kR) or punishment (kP), to physical (kEp) or mental (kEm) effort, and the impact of physical fatigue (kFp) or mental learning progress over time (kLm), along with a general bias to select the high efforts (bias). This approach aligns with previous studies that

have shown the efficacy of computational methods in deepening our understanding of behavioral mechanisms and uncovering neurobiological correlates otherwise not observable [2,43,44]. Adhering to established best practices in computational modeling [45], we first verified whether our behavioral parameters were recoverable using simulations (**Fig. 3a**) and then confirmed that parameters were not confounded with each other (**Fig. 3b**). Parameter recovery, assessed by comparing simulation parameters with those optimized, was successful in more than 80% of simulations for all the parameters, except for kLm which was recovered in 46% of simulations, a still rather reasonable result (**Fig. 3a**). No spurious correlations ($-0.5 < r < 0.5$) were detected between parameters (**Fig. 3b**), allowing for independent and sensitive recovery of each of the seven parameters (Palminteri et al., 2017). This indicates that our model was capable of independently and sensitively recovering each of the seven parameters.

Further validation was performed by challenging our behavioral model against variants with fewer parameters (**Fig. S4**). Model comparisons unanimously highlighted the importance of all the extracted parameters (i.e., kR, kP, kEm, kEp, kLm, kFp, and bias) in describing participants' behavior, despite the penalization for the added complexity of each additional parameter in the comparison process. Importantly, our model closely mirrored participant choices (median absolute error of 17.8 ± 6%, goodness-of-fit $R^2 = 0.56$) (**Fig. 3c-d**), effectively capturing the tendency of participants to choose more effortful options when monetary incentives were higher or the associated effort was less demanding.

dmPFC/dACC Metabolites Specifically Explain Sensitivity to Mental Effort

Next, we sought to determine whether dmPFC/dACC metabolites could explain any of the five idiosyncratic parameters characterizing HME modeling, derived from the computational modeling above. Specifically, we applied a separate XGBoost regression model to each parameter to investigate their predictability based on metabolite concentrations. Given that cognitive effort is often perceived as aversive, which influences action avoidance [47], we initially focused on sensitivity to mental effort (kEm) from metabolite concentrations. The dataset was split into 80% for training/validation (N=53) and 20% for testing (N = 14), with hyperparameter tuning conducted using *hyperopt* and CVLOO. The model showed a good level of accuracy in predicting kEm (range = 2.13, train RMSE = 0.16, validation RMSE = 0.42), and the test set yielded a modest prediction error (test RMSE = 0.4, $r = 0.56$, $p = 0.037$) (**Fig. 4a**), accounting for 30% of kEm's variance. This was confirmed by a permutation test, which indicated predictions significantly above chance level (95th percentile = 0.45 > model RMSE = 0.4) **(Fig. 4b**). Notably, training a model to predict other parameters involved in mental-effort decision making

such as reward sensitivity (kR), punishment sensitivity (kP), mental learning progress(kLm), and bias resulted in none significant predictions (all p>0.2).

To elucidate the impact of the five metabolites identified through our feature selection on kEm prediction, we examined their SHAP values (**Fig. 4c**). This analysis highlighted aspartate and lactate as the most discriminating features. Notably, aspartate exhibited a positive linear correlation with kEm ($r = 0.42$, $p = 0.0003$) (**Fig. S5b**). Although lactate was the second most important feature, it alone did not correlate linearly with kEm ($r = 0.063$, $p = 0.62$).

Refining the Model Explaining Mental Effort Decision-Making with Essential Biomarkers

So far, our work has yielded two effective XGBoost models for HME and kEm, utilizing 9 and 5 dmPFC/dACC metabolites, respectively. In our quest to unravel the neurometabolic foundations of motivation for mental effort, we next focused on further embracing parsimony. Given that overly complex models could hinder understanding and generalizability, our goal was to refine our models to strike a balance between simplicity and explanatory power [48]. Thus, we aimed to develop a streamlined model with a minimal, yet effective, set of features. This strategy is consistent with the established approaches in cognitive neuroscience and machine learning, where impactful models typically achieve high predictive accuracy with as few parameters as necessary [49].

First, we could explain HME robustly using a select few key metabolites. However, simply choosing the top two (i.e., glutamate and lactate; **Fig. S6a-c**) or top three (i.e., glutamate, lactate, and glutamine; **Fig. S6d-f**) predictors from our SHAP analysis for HME did not yield a significant prediction.

Inspired by the growing attempts to integrate biological context in machine learning in order to enhance model relevance and interpretability [50], we examined metabolic overlap among the top metabolites identified. Taking into account that Asp ranked top in the kEm model but rather low in the HME model, possibly due to its biosynthetic relationship with Glu and Gln [51] [and given that that these three metabolites are intertwined in the TCA cycle (**Fig. 5**)], we hypothesized that machine learning's tendency to minimize correlated features might have undervalued Asp's contribution in the HME model. Our data confirmed significant intercorrelations among these metabolites (**Fig. S5g**), suggesting that Asp, despite its lower ranking, could still hold unique predictive information. Notably, Lac, with no strong association with either Glu ($r = 0.03$, $p = 0.77$) or Asp ($r = 0.19$, $p = 0.11$), maintained its distinct variance. This led us to re-evaluate the potential of Glu, Asp, and Lactate concentrations in the dmPFC/dACC for predicting HME and their role as biomarkers for mental effort decision-making.

Thus, we trained again an XGBoost model and used again a train/validation/test analysis design with a CVLOO design. Data were split into training/validation into an 80% ratio, creating training/validation

(N =55) and testing (N = 14) data sets. To fit a linear response function to HME, we used XGBoost and the RMSE as a metric of error percentage. The model resulted in a good fit on the training (RMSE = 0.34%) and validation (RMSE = 15.94%) sets. (**Fig. 6a,b**) and a consistent result in our unbiased model estimate, the test set (RMSE = 11.4%, r = 0.64, p = 0.014), explaining up to 40% of the variance (**Fig. 6c**). The permutation test with 5000 permutations confirmed that our model's predictions significantly exceeded chance levels (95th percentile = 13.46 > model RMSE = 11.68). The results support the idea that a machine learning model based on a few dmPFC/dACC metabolite concentrations can predict participants' willingness to perform mental effort.

Analyzing the impact of glutamate, aspartate, and lactate on the model's prediction of HME using SHAP values revealed complex relationships, similar to our results from our initial model predicting HME. Specifically, glutamate and lactate did not exhibit linear correlations with HME (glutamate: r = -0.19, p = 0.12; lactate: r = -0.13, p = 0.27). Notably, extreme glutamate values were negatively associated with HME, still suggesting a quadratic relationship. In contrast, aspartate showed a strong negative linear correlation with HME (r = -0.37, p = 0.0018) (**Fig. S5a**).

Plasma and brain metabolite concentrations

Next, in order to explore if there is a relationship between our top identified metabolites in dmPFC/dACC predictive of HME with relevant plasma components, we examined if plasma concentrations of glutamate, aspartate, and lactate correlate with their levels in the dmPFC/dACC (**Fig. 7**). Furthermore, we also examined if plasma concentrations of glutamine correlated with its dmPFC/dACC counterpart levels, as glutamate is present in much lower concentrations than its precursor in blood [52]. We also performed the same analyses for the AI (our comparison brain region). Our analyses revealed no significant correlation between the plasma and dmPFC/dACC or AI concentrations of glutamate and aspartate. Interestingly, lactate displayed region-specific correlations, being significant in the dmPFC/dACC (r = 0.27, p = 0.023) but not in the AI (r = 0.14, p = 0.36). Conversely, glutamine showed a strong positive association in both brain regions (r = 0.54, p = $1.5 \cdot 10^{-5}$ in dmPFC/dACC; r = 0.34, p = 0.014 in AI), indicating a more global brain-plasma relationship.

Discussion

Differences in individuals' willingness to undertake incentivized effortful tasks can profoundly influence their life trajectories [3–5,53]. While regions such as the dmPFC/dACC and the AI are recognized within a network implicated in effort-based decision-making [2,8,9,11,12,14,54], the specific neurobiological factors driving individual differences in this domain are not well understood. Our study addresses this

knowledge gap by identifying key neurometabolic factors in the dmPFC/dACC that account for individual variability in the decision to exert mental effort.

Departing from earlier studies primarily focusing on individual metabolites [32,34,39,40,55,56], our multivariate approach yields a more comprehensive understanding of neurometabolic processes in mental effort-based decision-making. The high-field (7T) ^{1}H-MRS was pivotal for its superior spectral resolution enabling the differentiation of key metabolites, including glutamate and glutamine, which, along with lactate, emerged as top discriminants in our model. However, attempts to model HPE from dmPFC/dACC metabolites and leverage AI metabolites for HME prediction were inconclusive, highlighting a unique neurometabolic role of the dmPFC/dACC in mental effort prediction. This specificity is remarkable considering the functional link between the dmPFC/dACC and the AI within the salience network [57–60], particularly on mental effort exertion [41]. Our study identifies aspartate and lactate in the dmPFC/dACC as crucial for predicting mental effort sensitivity (kEm), with their increased levels corresponding to greater aversion to mental effort. Notably, kEm was the only motivational component predictable from our task, suggesting that sensitivity to mental effort is a key cognitive process influenced by dmPFC/dACC metabolism in mental effort-based decision-making. Furthermore, our refined machine learning model, designed to balance simplicity with explanatory power while incorporating biological context, highlights the combined roles of glutamate, aspartate, and lactate in the dmPFC/dACC as key discriminants for HME propensity, accounting for up to 40% of HME variance. Overall, our findings emphasize the collective significance of these metabolites in the dmPFC/dACC, offering new insights into the neurobiology of motivation for mental effort.

Glutamate, aspartate, and lactate are central to brain metabolism, playing crucial roles in supporting physiological functions critical for cognitive processes [37,38,61]. These metabolites, interconnected through the tricarboxylic acid (TCA) cycle and glycolysis (see **Fig. 5**) [62–64], underpin neuronal energy supply, neurotransmission, and amino acid synthesis [62,65,66]. The combined role of these three metabolites in predicting HME suggests that their interplay within the dmPFC/dACC fine-tunes neural computations related to mental effort feasibility and desirability.

Specifically, the neurometabolic profile in the dmPFC/dACC predictive of low mental effort exertion, involving combinations of elevated levels of glutamate, aspartate, and lactate, suggests a metabolic imbalance potentially indicative of mitochondrial dysfunction [67–69]. Such dysfunction could signal a disruption in the TCA cycle, as suggested by elevated aspartate and glutamate levels [70], and a compensatory shift towards glycolysis due to impaired oxidative phosphorylation, indicated by increased lactate levels. These disturbances may impair ATP production, amino acids, nucleotides, and bioactive molecules synthesis, essential for neuronal integrity and function [26,27], as well as

neurotransmitter synthesis and signaling pathways [71]. Mitochondrial dysfunction, evidenced in rodent models affecting demanding behavioral tasks [26,72,73], and metabolic imbalances within the dmPFC/dACC may directly affect energy-intensive cognitive tasks and decision-making processes, further diminishing motivation and cognitive control mechanisms.

In addition, inspecting the weights of these metabolites within the model further underscores insights into their potential contributions, particularly through the observed quadratic association of glutamate with mental effort choices and the strong negative linear correlation of aspartate with high mental effort (HME) choices. In agreement with evidence that low and high glutamate concentrations can impair cellular functions [74] and are implicated in cognitive deficits [75,76], glutamate's concentration within an optimal range -but not too high or too low- seems essential for high mental effort exertion in our study. Importantly, prefrontal glutamate levels can be increased by stress [77,78] and accumulate during prolonged high-demand tasks [34], reinforcing the relevance of glutamate dynamics in cognitive processes. This is consistent with findings showing increased glutamate levels in the dmPFC/dACC in response to cognitive demands [79,80], thus supporting our model's implications regarding glutamate's role in HME. Aspartate's negative association with HME choices and its link to reduced cognitive efficiency during effortful tasks highlight its significant, yet previously underappreciated, role in cognitive metabolism and neuronal activity. Lactate's contribution to HME and mental effort sensitivity (kEm) becomes evident in the multivariate context, with its high levels potentially reducing HME choices through mechanisms that extend beyond its traditional role as an energy substrate [81]. Lactate levels in the brain increase following systemic physiological changes, such as during intense exercise [82,83], and elevated levels are found in pathologies like schizophrenia and depression [84–87], which include motivational deficits as one of their core symptoms [53].

Of note, while metabolite levels in the brain, including those in the dmPFC/dACC, often exhibit remarkable stability over time [88–90], indicating distinct neuro-metabolic phenotypes [91], they are still susceptible to change. For example, external factors such as stress can dynamically alter glutamate levels in the prefrontal cortex [78,92], thereby influencing decision-making processes [93,94]. This highlights potential intervention targets for conditions characterized by motivational deficits. Our findings indicate that the brain concentrations of glutamate and aspartate are largely independent of their plasma levels, consistent with previous findings indicating that plasma glutamate concentrations contribute minimally to brain levels of this metabolite [52]. In contrast, a positive correlation between plasma and dmPFC/dACC lactate concentrations was observed, underscoring the unique transport dynamics of these metabolites across the blood-brain barrier [95,96]. Thus, while the direct influence of peripheral interventions on brain concentrations of glutamate and aspartate appears limited, the correlation between plasma and dmPFC/dACC lactate concentrations suggests that systemic changes

could impact brain metabolism and motivated behavior. Interventions aimed at modulating the gut microbiome or dietary supplements could thus offer indirect pathways to influence these critical metabolites, thereby impacting motivation and cognitive engagement.

While our study presents significant insights, it also has certain limitations. Although the models developed for HME and kEm were able to result in significant and robust predictions, they were trained on a limited sample size. Note, however, that the recruitment and testing of 75 subjects in the demanding 7T experimental studies represent a considerable sample size according to field standards. Moreover, the robustness and reliability of our findings as the model's predictions were validated using permutation tests. In the future, it will be important to benchmark the prediction capacity of our model and show its generalization capacity to both new datasets and other mental effort paradigms.

In conclusion, our study critically advances the understanding of neurometabolism in cognitive neuroscience, particularly in relation to motivated behavior. By demonstrating the combined predictive role of glutamate, aspartate, and lactate in the dmPFC/dACC, we uncover their collective capacity to predict mental effort in healthy individuals. This research not only bridges the gap between metabolic processes and cognitive function but also introduces a novel approach using machine learning to assess the collective impact of multiple metabolites. The insights gained provide a foundation for future investigations, potentially using animal models for causal analysis, and position these dmPFC/dACC metabolites as biological signatures for mental effort and motivation.

Acknowledgments

We thank the nursing staff at EPFL-Point Santé (Viviane Depuydt-Linder and Chiyama Mathivathanasekaram) and Centre Medical des Arcades (Lausanne), as well as members of the EPFL-LGC laboratory for their support in blood collection and processing. We thank Antonius Wiehler, Alizée Lopez-Persem and Bogdan Draganski for their inputs to the behavioral experimental design, and Olivier Ciclet (Nestlé Research), Adrien Frezal (Nestlé Research), and Irina Monnard (Nestlé Research) for their contributions to the plasma analyses.

Funding

Novartis Foundation for Medical-Biological Research grant 21B110 (NC)

Swiss National Science Foundation grant CRSII5_183564 (CS)

Swiss National Science Foundation grant 10531C_ 212914 (CS)

Foundation for the Encouragement of Nutrition Research in Switzerland (SFEFS) grant 607 (NC)

European Union's Horizon 2020 Research and Innovation Program (Marie Sklodowska-Curie) grant 101032219 (NC)

Intramural funding from the EFPL (C.S.)

Conflict of interest

JPG and BC are employees of Société des Produits Nestlé SA. C.S. is a member of the scientific advisory board of Amazentis/Timeline S.A and consults for Vandria S.A.

Declaration of generative AI and AI-assisted technologies in the writing process

During the preparation of this work the authors used ChatGPT 4.0 (OpenAI, San Francisco, California, USA) in order to correct and improve English quality of the manuscript. After using this tool/service, the authors reviewed and edited the content as needed and take full responsibility for the content of the publication.

Figure Legends

Fig. 1: Overview of experimental design. (**a-b**) Localization of dmPFC/dACC and AI voxels (20 x 20 x 20mm^3) targeted for ^{1}H-MRS acquisitions. The voxels are displayed in coronal and sagittal sections, overlaid on the MNI152 T1 average anatomical scan for reference. (**c**) Example of a ^{1}H-MR spectrum obtained from the dmPFC/dACC. The spectrum showcases the LGCModel spectral fit, macromolecular signals, baseline, residual fit, and individual metabolite fits for glutamate (Glu), aspartate (Asp), and lactate (Lac). (**d-e**) Effort-based decision-making tasks. Participants choose between options varying in effort and monetary incentive (reward or punishment) levels, with the potential for higher effort leading to greater rewards or avoiding larger punishments. Each trial started with a fixation cross, followed by a 5-seconds window where participants had to pick up the option that looked the more interesting for them based on their subjective preferences. There was always one option associated to a low effort and a low monetary incentive, while the other was associated to a larger monetary incentive but also to a higher effort. Physical and mental efforts were segregated into distinct blocks (2 for each type of effort), while rewards and punishment incentives were intermixed across trials within each block. After the choice was made, the chosen option was briefly displayed, followed by another fixation cross with a jitter to separate decision-making from the effort phase. (**d**) In the mental effort task, participants aimed to achieve a target number of correct responses within 10 seconds, determined by their prior calibration and the selected effort level. (**e**) In the physical effort task, participants had to maintain force above 55% of their maximal force for a duration depending on the chosen effort level (between 0.5 and 4.5s). Each trial ended with performance feedback indicating how much money was earned (or lost respectively) in the current trial.

Fig. 2: Analysis of models' explanations for physical and mental effort choices based on metabolite concentrations in dmPFC/dACC and AI. (**a**) Analysis of high physical effort (HPE) explanations using dmPFC/dACC metabolite concentrations with an XGBoost model indicates a moderate correlation not reaching significance ($r = 0.22$, $p = 0.22$) for the test set. (**b**) Furthermore, a permutation test indicated lack of predictive robustness (95th percentile threshold = 17.38% vs. model RMSE = 23.00). (**c**), For high mental effort (HME) choices, our model showed a strong correlation ($r = 0.56$, $p = 0.02$), underscoring the model's efficacy in anticipating decision patterns based on dmPFC/dACC metabolite profiles. (**d**) Permutation test for HME predictions confirms model accuracy (95th percentile threshold = 13.72% vs. model RMSE = 12.37%). (**e**) Feature importance analysis via SHAP values for HME prediction identifies nine key metabolites: glutamate (Glu), lactate (Lac), glutamine (Gln), taurine (Tau), N-acetylaspartate (NAA), N-acetylaspartylglutamate (NAAG), aspartate (Asp), glutathione (GSH), and creatine (Cr). (**f**) A model trained on AI metabolites' predictive power for HME reveals a negative correlation between

predicted and actual HME that does not reach statistical significance (r = -0.47, p = 0.06). (**g**), A permutation test further indicates a significant deviation in model performance for AI-based predictions (95th percentile threshold = 13.89% vs. model RMSE = 23.28%), highlighting a failure to predict HME choices based on AI metabolites.

Fig. 3: Comprehensive analysis of model parameters. (**a**) Confusion matrix evaluating the model's parameter recovery capability, contrasting recovered parameters against their original (simulated) counterparts. The parameters correspond to the sensitivity for reward (kR), punishment (kP), physical effort (kEp), mental effort (kEm), a bias toward the high effort option (bias), physical fatigue (kFp) and mental learning (kLm). (**b**) Autocorrelation matrix derived from 30'000 simulations assessing the identifiability of all model parameters. (**c**) Heatmap representing the percentage of high mental effort (HME) choices in function of the difference between the high and the low effort option in terms of effort and incentive levels across participants. (**d**) Corresponding heatmap representing the percentage of high mental effort (HME) choices predicted by our computational model in function of the difference between the high and the low effort option in terms of effort and incentive levels.

Fig. 4: Assessment of the model's explanatory power for mental effort sensitivity (kEm) using dmPFC/dACC metabolite concentrations. (**a**) A model based on dmPFC/dACC metabolites selected through an automated feature selection process shows a positive correlation (r = 0.56, p = 0.018) between predicted and observed values of kEm based on the XGBoost model's test set performance, highlighting the model's predictive accuracy. (**b**) Histogram of root mean square error (RMSE) from a permutation test involving random label permutation showing a clear validation of the model's robustness. The test, and the results show the model's RMSE (0.4) surpassing the 95th percentile of the permuted data (threshold RMSE = 0.45), confirming that the model's predictive success is not due to chance. (**c**) SHAP summary plot representing the impact of each feature on the model output for individual predictions. The analysis identifies five key metabolite parameters—Aspartate (Asp), Lactate (Lac), Glutathione (GSH), Glutamine (Gln), and the Glutamine/Glutamate (Gln/Glu) ratio—. Right panel: The horizontal dispersion of SHAP values per feature indicates the variability and influence of each on model predictions.

Fig. 5: Schematic representation of the identified metabolites within the tricarboxylic acid (TCA) cycle and the malate-aspartate shuttle (MAS) within mitochondria. The scheme depicts the interplay among key metabolites pertinent to neuronal energy metabolism. Highlighted in bold purple are the key metabolites related to mental effort motivation identified in this study: glutamate (Glu), aspartate (Asp), and lactate (Lac). The diagram traces the pathways of Asp and Glu within the TCA cycle and the

role of Lac in glycolysis. Key intermediates include pyruvate (Pyr), alpha-ketoglutarate (α-KG), oxaloacetate (OAA), malate (Mal), and acetyl-CoA, along with the redox couple NAD+/NADH, integral to both the TCA cycle and MAS. This visual abstract underscores the metabolic fluxes that are hypothesized to underpin the cognitive processes.

Fig. 6: Model for high mental effort (HME) choices using key metabolites from the dmPFC/dACC. (**a**) A strong positive correlation ($r = 0.64$, $p = 0.007$) between the XGBoost model's predicted probability of HME choices and the observed percentages within the test set, indicating robust predictive validity using the metabolites glutamate (Glu), aspartate (Asp), and lactate (Lac). (**b**) A permutation test that randomizes the labels and recalculates the RMSE to compare against the model's true performance indicates the model's predictive reliability, i.e., the true RMSE of the model (11.68%) is well below the 95th percentile of the permuted distribution (threshold RMSE = 13.46%), indicating that the model's predictions are not due to random chance. (**c**) SHAP value summary plot depicting the impact of each metabolite on the model's predictions for individual subjects. Right panel: The magnitude and distribution of the SHAP values for glutamate, aspartate, and lactate indicate their respective contributions to the model's decision-making process.

STAR★Methods

Experimental model and subject details

Participants

The results presented in this study are part of a broader study investigating inter-individual differences in motivated behavior. Here, we focused on a subset of data related to metabolite concentrations and behavioral measures.

A total of 75 healthy right-handed volunteers (40 females) participated in this study, approved by the Cantonal Ethics Committee of Vaud (CER-VD), Switzerland. Recruitment was through the Université de Lausanne (UNIL) LABEX platform and local advertisements. Fluency in French (minimum B2 level) was a requirement. Exclusion criteria included being outside the 25 - 40 years age range, regular drug or medication use, history of neurological disorders, and MRI contraindications (e.g., pregnancy, claustrophobia, tattoos near the neck, or metallic implants). Informed consent was obtained from all participants before being invited to the study. Pre-visit, online questionnaires were completed, including the Montgomery Asberg Depression Rating Scale – self-rated (MADRS-S), with a cutoff of 4 differentiating non-depressive from mild/high depressive individuals. This ensured a wide behavior range and sufficient inter-individual variability. Two participants were excluded due to incomplete behavioral experiments, and four due to consistently choosing the effortful option, leaving a final sample of 69 subjects (34 females; mean age = 30.5 ± 3.9 years; mean weight = 67.9 ± 12.6 kg; mean BMI = 22.8 ± 3.1) for our first and third machine learning models. For the second model, after excluding 2 additional participants for aberrant behavioral parameter values, the final sample comprised 67 subjects (34 females; mean age = 29.9 ± 3.9 years; mean weight = 67.7 ± 12.5 kg; mean BMI = 22.8 ± 3).

Compensation included a base payment of 70 CHF, an additional 10 CHF per experiment hour, and a fixed amount of 4 CHF for each time they performed a physical or mental maximal performance, completed ten times. Indifference point measurements and task performance also contributed to earnings (see Supplementary Material), averaging 204 ± 17.4 CHF per participant.

Method details

Experimental procedure

The study began uniformly at 2 pm to control for circadian rhythm effects. Participants abstained from eating for 1.5 hours before attendance. Blood samples were collected by healthcare professionals at specified locations (i.e., Point Santé" in EPFL and the "Centre Médical des Arcades", Lausanne) followed by baseline metabolite concentration assessments using proton magnetic resonance

spectroscopy (^{1}H-MRS) in the dmPFC/dACC and AI (see Fig. 1a-c). Task training occurred outside the scanner, with participants' maximum voluntary contraction (MVC) and maximum number of correct responses (MNCR) determined to calibrate task difficulty. The range of incentives used was calibrated by identifying the indifference points, corresponding to a 50% chance of accepting a certain level of effort for a given monetary incentive [97]. The behavioral task explores different aspects of motivated behavior while capturing a wide range of interindividual differences (Fig. 1d). On every trial, participants were asked to choose between a fixed low incentive/low effort option and a high incentive/high effort option, varying in both effort and incentive levels. After their choice selection, the selected option was displayed by continuous (for high confidence) or dotted (for low confidence) lines reflecting the level of confidence indicated by the subject. After their choice, participants had to perform the corresponding effort chosen. Incentives were either framed as monetary loss or gain. Effort was either physical, implying to exert a force equal or superior to 55 % of the participant's MVC during a varying amount of time depending on the level of effort selected, or mental, implying to perform different numbers of correct responses in a 2-back task, depending on their MNCR. The complete set of explanations is reported in the Supplementary Materials.

MRS acquisition and preprocessing

Proton magnetic resonance (^{1}H-MR) spectra were collected using a 7 Tesla/68 cm MR scanner (Magnetom, Siemens Medical Solutions, Erlangen, Germany) with a single-channel quadrature transmitter and a 32-channel receive coil (Nova Medical Inc., MA, USA). To optimize the magnetic field homogeneity, shimming was performed using FAST(EST)MAP [98] for both first and second-order. All 1H MR spectra were acquired using Semi-adiabatic spin echo full intensity acquired localized (sSPECIAL) [99,100] with the following parameters: TE/TR = 16/5000ms, 2 averages, VOI = 20 x 20 x 20 mm for dmPFC/dACC and 20 x 20 x 20 mm for AI dmPFC/dACC. All spectra were corrected for frequency/phase shifts and averaged. LCModel was used for spectral fitting and metabolite quantification [101] with a basis set that included simulated metabolite spectra and an experimentally measured macromolecule baseline. An unsuppressed water spectrum was acquired and used as an internal reference for metabolite quantification in LCModel.

T1-weighted images were acquired by MP2RAGE and used to calculate the tissue composition within the MRS voxel. The T1-weigthed images were then segmented into grey matter (GM), white matter (WM), and cerebrospinal fluid (CSF) in SPM12 toolbox (Wellcome Trust Center for NeuroImaging, London, UK) with the MarsBaR package (https://marsbar-toolbox.github.io/) [102], creating the VOI mask for the MRS voxel. Metabolite concentrations were adjusted for the CSF fraction, assuming water concentrations of 43,300 mM in GM, 35,880 mM in the WM, and 55,556 mM in the CSF. In

addition, to ensure all voxels were positioned correctly, we computed a density map of metabolites measurement, highlighting the precision of our voxel positioning, based on our MP2RAGE image and VOI mask (Fig. S7).

Following metabolite quantification in LCModel and correction, any computed metabolite concentrations with a Cramér-Rao lower bounds (CRLB) higher than 50 % were rejected. In addition, any participants with metabolite concentrations higher than the mean ± 3SD were removed as outliers. Then, the metabolite ratios were computed, namely glutamine to glutamate (Gln/Glu) and glutamate to γ-aminobutyric acid (Glu/GABA). Finally, using the Python package sklearn.*IterativeImputer*, the missing dataset values were filled by multivariate imputation.

Quantification and Statistical Analysis

Computational modeling of motivated behavior

Participants' choices were fitted with a softmax model using Matlab's VBA toolbox (https://mbb-team.github.io/VBA-toolbox/) which implements Variational Bayesian analysis under the Laplace approximation [103]. The algorithm provides an estimate of the posterior density over the model parameters, starting from Gaussian priors.

We compared five models individually across each subject, each increasing in complexity (Fig. S3). In our models, we modeled the complete behavior of participants in order to compare physical and mental effort types. Confidence was included to improve behavior computation modeling accuracy. To reduce the risk of overfitting, and improve robustness, all models' components were kept linear. By assessing how each model accounted for each participant's choice we captured seven different components of motivated behavior, namely sensitivity to reward (kR), punishment (kP), physical (kEp) and mental effort (kEm), physical fatigue (kFp) and mental learning progress (kLm), and a bias term (bias). These sensitivities were used to compare subjective values across options. We found that participants' choices were best predicted by our fifth model (Fig. S3), composed as follows:

$$\Delta SV(t) = kR * \Delta R(t) * idx_I + kP * \Delta P(t) * (1 - idx_I) - \Delta Ep(t) * (kEp + kFp * \sum_{t=0}^{T} AUC(t)) * idx_E - \Delta Em(t) * \left(kEm + kFm * \frac{N_{correct\ answers}(t-1)}{effort\ time(t-1)}\right) * (1 - idx_E) \quad (1)$$

Where ΔSV is the subjective value of the varying option discounted by the subjective value of the fixed option (1). ΔR and ΔP represent the difference in the monetary incentives (reward or punishment) between the varying option and the fixed option, idx_I is a binary representation of the incentive condition of the current trial (reward or punishment), ΔE represents the difference in effort level between the varying option and the fixed option, idx_E is a binary representation of the effort type of the current block (physical or mental), the area under the curve (AUC) represents the total force

exerted in a given trial during a physical block, $N_{correct\ answers}$(t-1) represents the number of correct answers provided in the previous trial and effort time(t-1) represents the time it took to complete the effort in the previous trial, during a mental block. When a block was specific to an effort type, or a trial specific to an incentive type, its counterpart was set to 0. Finally, ΔSV is then taken as input in a *softmax* function:

$$P_{High\ effort}(t) = \frac{1}{1+e^{-\Delta SV(t)+bias}} \qquad (2)$$

Where $P_{High\ effort}(t)$ represents the probability of choosing the high effort/high incentive option for a given ΔSV at trial t (2). Apart from the bias parameter (*bias*), all parameters were positively constrained through a log(1+exp(x)) transformation. With variables to fit with low values, selected priors were attributed with a null mean, and a sigma set to 100 for kR and kP to account for high fluctuations in ΔI between participants due to IP calibration and forced positivity, and set to 1 for all other parameters. Finally, apart from the bias, parameters were boxcox transformed to reduce skewness and increase normality [104].

Feature selection and extreme gradient boosting trees (XGBoost).

Feature selection plays a crucial role in developing predictive models, as it simplifies the model by removing redundant features and mitigates overfitting, particularly for small sample sizes with limited generalization ability. Our dataset was first divided in a train/test split, with 80% of the dataset kept for training and 20% for testing. To avoid bias in test predictions, feature selection was conducted on the training dataset for both models. Features with a Pearson correlation coefficient smaller than 0.1 with the target variable were removed. As a second round of feature selection, Sklearn.*AdaBoostRegressor* package was used to train models using approach CVLOO to predict target variables. The selected features were those that yielded the smallest validation error from the CVLOO approach. The resulting metabolites were used to train both machine learning algorithms.

We employed *XGBoost* to predict the number of high-effort options performed by participants (models 1 and 3) and the mental effort perception, extracted with the behavioral model (model 2) using a selected set of metabolite concentrations. We used the *XGBRegressor* function from the Python *XGBoost* package to fit both models. XGBoost includes several adjustable hyperparameters. We optimized the step size shrinkage (eta), maximum depth of the tree (max_depth), minimum sum of instance weight (min_child_weight), and regularization parameters (gamma, lambda, alpha) through Bayesian optimization with the *hyperopt* Python package and CVLOO [105]. We assessed our model's prediction performance by correlating the predicted and true values of the target variables in a holdout sample that was not utilized in the model learning process. The train and test datasets were

loaded into data frames using the *pandas* Python package and evaluated using model assessment metrics computed with the *numpy* Python package. Additionally, we computed the SHAP values using the *shap* Python package [106].

References

1. Chong, T.T.-J., Bonnelle, V., and Husain, M. (2016). Quantifying motivation with effort-based decision-making paradigms in health and disease. In Progress in Brain Research (Elsevier), pp. 71–100. 10.1016/bs.pbr.2016.05.002.

2. Pessiglione, M., Vinckier, F., Bouret, S., Daunizeau, J., and Le Bouc, R. (2018). Why not try harder? Computational approach to motivation deficits in neuro-psychiatric diseases. Brain *141*, 629–650. 10.1093/brain/awx278.

3. Duckworth, A.L., Eichstaedt, J.C., and Ungar, L.H. (2015). The Mechanics of Human Achievement: Newtonian Model of Achievement. Soc. Personal. Psychol. Compass *9*, 359–369. 10.1111/spc3.12178.

4. Epstein, J., and Silbersweig, D. (2015). The Neuropsychiatric Spectrum of Motivational Disorders. J. Neuropsychiatry Clin. Neurosci. *27*, 7–18. 10.1176/appi.neuropsych.13120370.

5. Kanfer, R., Frese, M., and Johnson, R.E. (2017). Motivation related to work: A century of progress. J. Appl. Psychol. *102*, 338–355. 10.1037/apl0000133.

6. Le Heron, C., Apps., M.A.J., and Husain, M. (2018). The anatomy of apathy: A neurocognitive framework for amotivated behaviour. Neuropsychologia *118*, 54–67. 10.1016/j.neuropsychologia.2017.07.003.

7. Bartra, O., McGuire, J.T., and Kable, J.W. (2013). The valuation system: A coordinate-based meta-analysis of BOLD fMRI experiments examining neural correlates of subjective value. NeuroImage *76*, 412–427. 10.1016/j.neuroimage.2013.02.063.

8. Clairis, N., and Lopez-Persem, A. (2023). Debates on the dorsomedial prefrontal/dorsal anterior cingulate cortex: insights for future research. Brain, awad263. 10.1093/brain/awad263.

9. Lopez-Gamundi, P., Yao, Y.-W., Chong, T.T.-J., Heekeren, H.R., Mas-Herrero, E., and Marco-Pallarés, J. (2021). The neural basis of effort valuation: A meta-analysis of functional magnetic resonance imaging studies. Neurosci. Biobehav. Rev. *131*, 1275–1287. 10.1016/j.neubiorev.2021.10.024.

10. Soutschek, A., Nadporozhskaia, L., and Christian, P. (2022). Brain stimulation over dorsomedial prefrontal cortex modulates effort-based decision making. Cogn. Affect. Behav. Neurosci. *22*, 1264–1274. 10.3758/s13415-022-01021-z.

11. Chong, T.T.-J., Apps, M., Giehl, K., Sillence, A., Grima, L.L., and Husain, M. (2017). Neurocomputational mechanisms underlying subjective valuation of effort costs. PLOS Biol. *15*, e1002598. 10.1371/journal.pbio.1002598.

12. Kurniawan, I.T., Grueschow, M., and Ruff, C.C. (2021). Anticipatory Energization Revealed by Pupil and Brain Activity Guides Human Effort-Based Decision Making. J. Neurosci. *41*, 6328–6342. 10.1523/JNEUROSCI.3027-20.2021.

13. Le Bouc, R., and Pessiglione, M. (2022). A neuro-computational account of procrastination behavior. Nat. Commun. *13*, 5639. 10.1038/s41467-022-33119-w.

14. Le Bouc, R., Borderies, N., Carle, G., Robriquet, C., Vinckier, F., Daunizeau, J., Azuar, C., Levy, R., and Pessiglione, M. (2023). Effort avoidance as a core mechanism of apathy in frontotemporal dementia. Brain *146*, 712–726. 10.1093/brain/awac427.

15. Darby, R.R., Joutsa, J., Burke, M.J., and Fox, M.D. (2018). Lesion network localization of free will. Proc. Natl. Acad. Sci. *115*, 10792–10797. 10.1073/pnas.1814117115.

16. Morella, I.M., Brambilla, R., and Morè, L. (2022). Emerging roles of brain metabolism in cognitive impairment and neuropsychiatric disorders. Neurosci. Biobehav. Rev. *142*, 104892. 10.1016/j.neubiorev.2022.104892.

17. Ülgen, D.H., Ruigrok, S.R., and Sandi, C. (2023). Powering the social brain: Mitochondria in social behaviour. Curr. Opin. Neurobiol. *79*, 102675. 10.1016/j.conb.2022.102675.

18. Yellen, G. (2018). Fueling thought: Management of glycolysis and oxidative phosphorylation in neuronal metabolism. J. Cell Biol. *217*, 2235–2246. 10.1083/jcb.201803152.

19. Baumeister, R.F. (2003). Ego depletion and self-regulation failure: a resource model of self-control. Alcohol. Clin. Exp. Res. *27*, 281–284. 10.1097/01.ALC.0000060879.61384.A4.

20. Gailliot, M.T., and Baumeister, R.F. (2007). The Physiology of Willpower: Linking Blood Glucose to Self-Control. Personal. Soc. Psychol. Rev. *11*, 303–327. 10.1177/1088868307303030.

21. Dang, J. (2016). Testing the role of glucose in self-control: A meta-analysis. Appetite *107*, 222–230. 10.1016/j.appet.2016.07.021.

22. Job, V., Walton, G.M., Bernecker, K., and Dweck, C.S. (2013). Beliefs about willpower determine the impact of glucose on self-control. Proc. Natl. Acad. Sci. *110*, 14837–14842. 10.1073/pnas.1313475110.

23. Lange, F., and Eggert, F. (2014). Sweet delusion. Glucose drinks fail to counteract ego depletion. Appetite *75*, 54–63. 10.1016/j.appet.2013.12.020.

24. Vadillo, M.A., Gold, N., and Osman, M. (2016). The Bitter Truth About Sugar and Willpower: The Limited Evidential Value of the Glucose Model of Ego Depletion. Psychol. Sci. *27*, 1207–1214. 10.1177/0956797616654911.

25. Devine, M.J., and Kittler, J.T. (2018). Mitochondria at the neuronal presynapse in health and disease. Nat. Rev. Neurosci. *19*, 63–80. 10.1038/nrn.2017.170.

26. Gebara, E., Zanoletti, O., Ghosal, S., Grosse, J., Schneider, B.L., Knott, G., Astori, S., and Sandi, C. (2021). Mitofusin-2 in the Nucleus Accumbens Regulates Anxiety and Depression-like Behaviors Through Mitochondrial and Neuronal Actions. Biol. Psychiatry *89*, 1033–1044. 10.1016/j.biopsych.2020.12.003.

27. Ghosal, S., Gebara, E., Ramos-Fernández, E., Chioino, A., Grosse, J., Guillot De Suduiraut, I., Zanoletti, O., Schneider, B., Zorzano, A., Astori, S., et al. (2023). Mitofusin-2 in nucleus accumbens D2-MSNs regulates social dominance and neuronal function. Cell Rep. *42*, 112776. 10.1016/j.celrep.2023.112776.

28. Lutas, A., and Yellen, G. (2013). The ketogenic diet: metabolic influences on brain excitability and epilepsy. Trends Neurosci. *36*, 32–40. 10.1016/j.tins.2012.11.005.

29. Morató, L., Astori, S., Zalachoras, I., Rodrigues, J., Ghosal, S., Huang, W., Guillot De Suduiraut, I., Grosse, J., Zanoletti, O., Cao, L., et al. (2022). eNAMPT actions through nucleus accumbens NAD^+/SIRT1 link increased adiposity with sociability deficits programmed by peripuberty stress. Sci. Adv. *8*, eabj9109. 10.1126/sciadv.abj9109.

30. Cherix, A., Larrieu, T., Grosse, J., Rodrigues, J., McEwen, B., Nasca, C., Gruetter, R., and Sandi, C. (2020). Metabolic signature in nucleus accumbens for anti-depressant-like effects of acetyl-L-carnitine. eLife *9*, e50631. 10.7554/eLife.50631.

31. Lapidus, K.A.B., Gabbay, V., Mao, X., Johnson, A., Murrough, J.W., Mathew, S.J., and Shungu, D.C. (2014). In vivo 1H MRS study of potential associations between glutathione, oxidative stress and anhedonia in major depressive disorder. Neurosci. Lett. *569*, 74–79. 10.1016/j.neulet.2014.03.056.

32. Strasser, A., Luksys, G., Xin, L., Pessiglione, M., Gruetter, R., and Sandi, C. (2020). Glutamine-to-glutamate ratio in the nucleus accumbens predicts effort-based motivated performance in humans. Neuropsychopharmacology *45*, 2048–2057. 10.1038/s41386-020-0760-6.

33. Wang, A.M., Pradhan, S., Coughlin, J.M., Trivedi, A., DuBois, S.L., Crawford, J.L., Sedlak, T.W., Nucifora, F.C., Nestadt, G., Nucifora, L.G., et al. (2019). Assessing Brain Metabolism With 7-T Proton Magnetic Resonance Spectroscopy in Patients With First-Episode Psychosis. JAMA Psychiatry *76*, 314. 10.1001/jamapsychiatry.2018.3637.

34. Wiehler, A., Branzoli, F., Adanyeguh, I., Mochel, F., and Pessiglione, M. (2022). A neuro-metabolic account of why daylong cognitive work alters the control of economic decisions. Curr. Biol. *32*, 3564-3575.e5. 10.1016/j.cub.2022.07.010.

35. Zalachoras, I., Ramos-Fernández, E., Hollis, F., Trovo, L., Rodrigues, J., Strasser, A., Zanoletti, O., Steiner, P., Preitner, N., Xin, L., et al. (2022). Glutathione in the nucleus accumbens regulates motivation to exert reward-incentivized effort. eLife *11*, e77791. 10.7554/eLife.77791.

36. Maddock, R.J., and Buonocore, M.H. (2012). MR spectroscopic studies of the brain in psychiatric disorders. Curr. Top. Behav. Neurosci. *11*, 199–251. 10.1007/7854_2011_197.

37. Rae, C.D. (2014). A guide to the metabolic pathways and function of metabolites observed in human brain 1H magnetic resonance spectra. Neurochem. Res. *39*, 1–36. 10.1007/s11064-013-1199-5.

38. Rae, C.D., Baur, J.A., Borges, K., Dienel, G., Díaz-García, C.M., Douglass, S.R., Drew, K., Duarte, J.M.N., Duran, J., Kann, O., et al. (2024). Brain energy metabolism: A roadmap for future research. J. Neurochem., jnc.16032. 10.1111/jnc.16032.

39. Jocham, G., Hunt, L.T., Near, J., and Behrens, T.E.J. (2012). A mechanism for value-guided choice based on the excitation-inhibition balance in prefrontal cortex. Nat. Neurosci. *15*, 960–961. 10.1038/nn.3140.

40. Yoon, J.H., Grandelis, A., and Maddock, R.J. (2016). Dorsolateral Prefrontal Cortex GABA Concentration in Humans Predicts Working Memory Load Processing Capacity. J. Neurosci. *36*, 11788–11794. 10.1523/JNEUROSCI.1970-16.2016.

41. Aben, B., Buc Calderon, C., Van den Bussche, E., and Verguts, T. (2020). Cognitive Effort Modulates Connectivity between Dorsal Anterior Cingulate Cortex and Task-Relevant Cortical Areas. J. Neurosci. Off. J. Soc. Neurosci. *40*, 3838–3848. 10.1523/JNEUROSCI.2948-19.2020.

42. Bonnelle, V., Veromann, K.-R., Burnett Heyes, S., Lo Sterzo, E., Manohar, S., and Husain, M. (2015). Characterization of reward and effort mechanisms in apathy. J. Physiol.-Paris *109*, 16–26. 10.1016/j.jphysparis.2014.04.002.

43. Corrado, G., and Doya, K. (2007). Understanding Neural Coding through the Model-Based Analysis of Decision Making: Figure 1. J. Neurosci. *27*, 8178–8180. 10.1523/JNEUROSCI.1590-07.2007.

44. Nassar, M.R., and Frank, M.J. (2016). Taming the beast: extracting generalizable knowledge from computational models of cognition. Curr. Opin. Behav. Sci. *11*, 49–54. 10.1016/j.cobeha.2016.04.003.

45. Wilson, R.C., and Collins, A.G. (2019). Ten simple rules for the computational modeling of behavioral data. eLife *8*, e49547. 10.7554/eLife.49547.

46. Palminteri, S., Wyart, V., and Koechlin, E. (2017). The Importance of Falsification in Computational Cognitive Modeling. Trends Cogn. Sci. *21*, 425–433. 10.1016/j.tics.2017.03.011.

47. Vogel, T.A., Savelson, Z.M., Otto, A.R., and Roy, M. (2020). Forced choices reveal a trade-off between cognitive effort and physical pain. eLife *9*, e59410. 10.7554/eLife.59410.

48. Vandekerckhove, J., Matke, D., and Wagenmakers, E.-J. (2015). Model Comparison and the Principle of Parsimony. In The Oxford Handbook of Computational and Mathematical Psychology.

49. Takahashi, Y., Ueki, M., Yamada, M., Tamiya, G., Motoike, I.N., Saigusa, D., Sakurai, M., Nagami, F., Ogishima, S., Koshiba, S., et al. (2020). Improved metabolomic data-based prediction of depressive symptoms using nonlinear machine learning with feature selection. Transl. Psychiatry *10*, 157. 10.1038/s41398-020-0831-9.

50. Zampieri, G., Vijayakumar, S., Yaneske, E., and Angione, C. (2019). Machine and deep learning meet genome-scale metabolic modeling. PLOS Comput. Biol. *15*, e1007084. 10.1371/journal.pcbi.1007084.

51. Holten, A.T., and Gundersen, V. (2008). Glutamine as a precursor for transmitter glutamate, aspartate and GABA in the cerebellum: a role for phosphate-activated glutaminase. J. Neurochem. *104*, 1032–1042. 10.1111/j.1471-4159.2007.05065.x.

52. Smith, Q.R. (2000). Transport of Glutamate and Other Amino Acids at the Blood-Brain Barrier. J. Nutr. *130*, 1016S-1022S. 10.1093/jn/130.4.1016S.

53. Husain, M., and Roiser, J.P. (2018). Neuroscience of apathy and anhedonia: a transdiagnostic approach. Nat. Rev. Neurosci. *19*, 470–484. 10.1038/s41583-018-0029-9.

54. Shenhav, A., Musslick, S., Lieder, F., Kool, W., Griffiths, T.L., Cohen, J.D., and Botvinick, M.M. (2017). Toward a Rational and Mechanistic Account of Mental Effort. Annu. Rev. Neurosci. *40*, 99–124. 10.1146/annurev-neuro-072116-031526.

55. Grachev, I.D., Kumar, R., Ramachandran, T.S., and Szeverenyi, N.M. (2001). Cognitive interference is associated with neuronal marker N-acetyl aspartate in the anterior cingulate cortex: an in vivo (1)H-MRS study of the Stroop Color-Word task. Mol. Psychiatry *6*, 496, 529–539. 10.1038/sj.mp.4000940.

56. Yücel, M., Harrison, B.J., Wood, S.J., Fornito, A., Clarke, K., Wellard, R.M., Cotton, S., and Pantelis, C. (2007). State, trait and biochemical influences on human anterior cingulate function. NeuroImage *34*, 1766–1773. 10.1016/j.neuroimage.2006.08.057.

57. Litt, A., Plassmann, H., Shiv, B., and Rangel, A. (2011). Dissociating Valuation and Saliency Signals during Decision-Making. Cereb. Cortex *21*, 95–102. 10.1093/cercor/bhq065.

58. Seeley, W.W., Menon, V., Schatzberg, A.F., Keller, J., Glover, G.H., Kenna, H., Reiss, A.L., and Greicius, M.D. (2007). Dissociable Intrinsic Connectivity Networks for Salience Processing and Executive Control. J. Neurosci. *27*, 2349–2356. 10.1523/JNEUROSCI.5587-06.2007.

59. Uddin, L.Q. (2015). Salience processing and insular cortical function and dysfunction. Nat. Rev. Neurosci. *16*, 55–61. 10.1038/nrn3857.

60. Uddin, L.Q., Yeo, B.T.T., and Spreng, R.N. (2019). Towards a Universal Taxonomy of Macro-scale Functional Human Brain Networks. Brain Topogr. *32*, 926–942. 10.1007/s10548-019-00744-6.

61. Li, J., Xia, Y., Xu, H., Xiong, R., Zhao, Y., Li, P., Yang, T., Huang, Q., and Shan, F. (2022). Activation of brain lactate receptor GPR81 aggravates exercise-induced central fatigue. Am. J. Physiol.-Regul. Integr. Comp. Physiol. *323*, R822–R831. 10.1152/ajpregu.00094.2022.

62. Waagepetersen, H.S., Bakken, I.J., Larsson, O.M., Sonnewald, U., and Schousboe, A. (1998). Metabolism of Lactate in Cultured GABAergic Neurons Studied by ^{13}C Nuclear Magnetic Resonance Spectroscopy. J. Cereb. Blood Flow Metab. *18*, 109–117. 10.1097/00004647-199801000-00011.

63. McKenna, M.C., Sonnewald, U., Huang, X., Stevenson, J., and Zielke, H.R. (1996). Exogenous Glutamate Concentration Regulates the Metabolic Fate of Glutamate in Astrocytes. J. Neurochem. *66*, 386–393. 10.1046/j.1471-4159.1996.66010386.x.

64. Schousboe, A., Scafidi, S., Bak, L.K., Waagepetersen, H.S., and McKenna, M.C. (2014). Glutamate Metabolism in the Brain Focusing on Astrocytes. In Glutamate and ATP at the Interface of Metabolism and Signaling in the Brain Advances in Neurobiology., V. Parpura, A. Schousboe, and A. Verkhratsky, eds. (Springer International Publishing), pp. 13–30. 10.1007/978-3-319-08894-5_2.

65. Juaristi, I., Contreras, L., González-Sánchez, P., Pérez-Liébana, I., González-Moreno, L., Pardo, B., del Arco, A., and Satrústegui, J. (2019). The Response to Stimulation in Neurons and Astrocytes. Neurochem. Res. *44*, 2385–2391. 10.1007/s11064-019-02803-7.

66. Pellerin, L., and Magistretti, P.J. (2012). Sweet Sixteen for ANLS. J. Cereb. Blood Flow Metab. *32*, 1152–1166. 10.1038/jcbfm.2011.149.

67. Bianchi, M.C., Sgandurra, G., Tosetti, M., Battini, R., and Cioni, G. (2007). Brain Magnetic Resonance in the Diagnostic Evaluation of Mitochondrial Encephalopathies. Biosci. Rep. *27*, 69–85. 10.1007/s10540-007-9046-z.

68. Nunnari, J., and Suomalainen, A. (2012). Mitochondria: In Sickness and in Health. Cell *148*, 1145–1159. 10.1016/j.cell.2012.02.035.

69. Schmiedel, J., Jackson, S., Schäfer, J., and Reichmann, H. (2003). Mitochondrial Cytopathies. J. Neurol. *250*, 267–277. 10.1007/s00415-003-0978-3.

70. Owen, O.E., Kalhan, S.C., and Hanson, R.W. (2002). The Key Role of Anaplerosis and Cataplerosis for Citric Acid Cycle Function. J. Biol. Chem. *277*, 30409–30412. 10.1074/jbc.R200006200.

71. Magistretti, P.J., and Allaman, I. (2015). A Cellular Perspective on Brain Energy Metabolism and Functional Imaging. Neuron *86*, 883–901. 10.1016/j.neuron.2015.03.035.

72. Hollis, F., Van Der Kooij, M.A., Zanoletti, O., Lozano, L., Cantó, C., and Sandi, C. (2015). Mitochondrial function in the brain links anxiety with social subordination. Proc. Natl. Acad. Sci. *112*, 15486–15491. 10.1073/pnas.1512653112.

73. van der Kooij, M.A., Hollis, F., Lozano, L., Zalachoras, I., Abad, S., Zanoletti, O., Grosse, J., Guillot de Suduiraut, I., Canto, C., and Sandi, C. (2018). Diazepam actions in the VTA enhance social dominance and mitochondrial function in the nucleus accumbens by activation of dopamine D1 receptors. Mol. Psychiatry *23*, 569–578. 10.1038/mp.2017.135.

74. Lau, A., and Tymianski, M. (2010). Glutamate receptors, neurotoxicity and neurodegeneration. Pflüg. Arch. - Eur. J. Physiol. *460*, 525–542. 10.1007/s00424-010-0809-1.

75. Shirayama, Y., Takahashi, M., Osone, F., Hara, A., and Okubo, T. (2017). Myo-inositol, Glutamate, and Glutamine in the Prefrontal Cortex, Hippocampus, and Amygdala in Major Depression. Biol. Psychiatry Cogn. Neurosci. Neuroimaging *2*, 196–204. 10.1016/j.bpsc.2016.11.006.

76. Nakahara, T., Tsugawa, S., Noda, Y., Ueno, F., Honda, S., Kinjo, M., Segawa, H., Hondo, N., Mori, Y., Watanabe, H., et al. (2022). Glutamatergic and GABAergic metabolite levels in schizophrenia-spectrum disorders: a meta-analysis of 1H-magnetic resonance spectroscopy studies. Mol. Psychiatry *27*, 744–757. 10.1038/s41380-021-01297-6.

77. Moghaddam, B. (2002). Stress activation of glutamate neurotransmission in the prefrontal cortex: implications for dopamine-associated psychiatric disorders. Biol. Psychiatry *51*, 775–787. 10.1016/S0006-3223(01)01362-2.

78. Sandi, C. (2011). Glucocorticoids act on glutamatergic pathways to affect memory processes. Trends Neurosci. *34*, 165–176. 10.1016/j.tins.2011.01.006.

79. Kühn, S., Schubert, F., Mekle, R., Wenger, E., Ittermann, B., Lindenberger, U., and Gallinat, J. (2016). Neurotransmitter changes during interference task in anterior cingulate cortex: evidence from fMRI-guided functional MRS at 3 T. Brain Struct. Funct. *221*, 2541–2551. 10.1007/s00429-015-1057-0.

80. Taylor, R., Schaefer, B., Densmore, M., Neufeld, R.W.J., Rajakumar, N., Williamson, P.C., and Théberge, J. (2015). Increased glutamate levels observed upon functional activation in the anterior cingulate cortex using the Stroop Task and functional spectroscopy. NeuroReport *26*, 107–112. 10.1097/WNR.0000000000000309.

81. Magistretti, P.J., and Allaman, I. (2018). Lactate in the brain: from metabolic end-product to signalling molecule. Nat. Rev. Neurosci. *19*, 235–249. 10.1038/nrn.2018.19.

82. Koush, Y., Rothman, D.L., Behar, K.L., De Graaf, R.A., and Hyder, F. (2022). Human brain functional MRS reveals interplay of metabolites implicated in neurotransmission and neuroenergetics. J. Cereb. Blood Flow Metab. *42*, 911–934. 10.1177/0271678X221076570.

83. Świątkiewicz, M., Gaździński, S., Madeyski, M., Kossowski, B., Langfort, J., Bogorodzki, P., Zawadzka-Bartczak, E., Sklinda, K., Walecki, J., and Grieb, P. (2023). Increased brain 1H-MRS

glutamate and lactate signals following maximal aerobic capacity exercise in young healthy males: an exploratory study. Biol. Sport *40*, 665–673. 10.5114/biolsport.2023.118335.

84. Ernst, J., Hock, A., Henning, A., Seifritz, E., Boeker, H., and Grimm, S. (2017). Increased pregenual anterior cingulate glucose and lactate concentrations in major depressive disorder. Mol. Psychiatry *22*, 113–119. 10.1038/mp.2016.73.

85. Machado-Vieira, R., Zanetti, M.V., Otaduy, M.C., De Sousa, R.T., Soeiro-de-Souza, M.G., Costa, A.C., Carvalho, A.F., Leite, C.C., Busatto, G.F., Zarate, C.A., et al. (2017). Increased Brain Lactate During Depressive Episodes and Reversal Effects by Lithium Monotherapy in Drug-Naive Bipolar Disorder: A 3-T 1H-MRS Study. J. Clin. Psychopharmacol. *37*, 40–45. 10.1097/JCP.0000000000000616.

86. Rowland, L.M., Pradhan, S., Korenic, S., Wijtenburg, S.A., Hong, L.E., Edden, R.A., and Barker, P.B. (2016). Elevated brain lactate in schizophrenia: a 7 T magnetic resonance spectroscopy study. Transl. Psychiatry *6*, e967–e967. 10.1038/tp.2016.239.

87. Soeiro-de-Souza, M.G., Pastorello, B.F., Leite, C.D.C., Henning, A., Moreno, R.A., and Garcia Otaduy, M.C. (2016). Dorsal Anterior Cingulate Lactate and Glutathione Levels in Euthymic Bipolar I Disorder: ^{1} H-MRS Study. Int. J. Neuropsychopharmacol. *19*, pyw032. 10.1093/ijnp/pyw032.

88. Lally, N., An, L., Banerjee, D., Niciu, M.J., Luckenbaugh, D.A., Richards, E.M., Roiser, J.P., Shen, J., Zarate, C.A., and Nugent, A.C. (2016). Reliability of 7T ^{1} H-MRS measured human prefrontal cortex glutamate, glutamine, and glutathione signals using an adapted echo time optimized PRESS sequence: A between- and within-sessions investigation: 7T ^{1} H-MRS Glutamatergic Reliability. J. Magn. Reson. Imaging *43*, 88–98. 10.1002/jmri.24970.

89. Ross, A.J., Sachdev, P.S., Wen, W., and Brodaty, H. (2006). Longitudinal Changes During Aging Using Proton Magnetic Resonance Spectroscopy. J. Gerontol. A. Biol. Sci. Med. Sci. *61*, 291–298. 10.1093/gerona/61.3.291.

90. Wang, M.-Y., Korbmacher, M., Eikeland, R., Craven, A.R., and Specht, K. (2024). The intra-individual reliability of 1 H-MRS measurement in the anterior cingulate cortex across 1 year. Hum. Brain Mapp. *45*, e26531. 10.1002/hbm.26531.

91. Wu, B., Bagshaw, A.P., Hickey, C., Kühn, S., and Wilson, M. (2022). Evidence for distinct neuro-metabolic phenotypes in humans. NeuroImage *249*, 118902. 10.1016/j.neuroimage.2022.118902.

92. Treccani, G., Musazzi, L., Perego, C., Milanese, M., Nava, N., Bonifacino, T., Lamanna, J., Malgaroli, A., Drago, F., Racagni, G., et al. (2014). Stress and corticosterone increase the readily releasable pool of glutamate vesicles in synaptic terminals of prefrontal and frontal cortex. Mol. Psychiatry *19*, 433–443. 10.1038/mp.2014.5.

93. Sanacora, G., Yan, Z., and Popoli, M. (2022). The stressed synapse 2.0: pathophysiological mechanisms in stress-related neuropsychiatric disorders. Nat. Rev. Neurosci. *23*, 86–103. 10.1038/s41583-021-00540-x.

94. Sandi, C. (2013). Stress and cognition. Wiley Interdiscip. Rev. Cogn. Sci. *4*, 245–261. 10.1002/wcs.1222.

95. Cruzat, V., Macedo Rogero, M., Noel Keane, K., Curi, R., and Newsholme, P. (2018). Glutamine: Metabolism and Immune Function, Supplementation and Clinical Translation. Nutrients *10*, 1564. 10.3390/nu10111564.

96. Hladky, S.B., and Barrand, M.A. (2016). Fluid and ion transfer across the blood–brain and blood–cerebrospinal fluid barriers; a comparative account of mechanisms and roles. Fluids Barriers CNS *13*, 19. 10.1186/s12987-016-0040-3.

97. Westbrook, A., van den Bosch, R., Määttä, J.I., Hofmans, L., Papadopetraki, D., Cools, R., and Frank, M.J. (2019). Dopamine Promotes Cognitive Effort by Biasing the Benefits Versus Costs of Cognitive Work (Neuroscience) 10.1101/778134.

98. Gruetter, R. (1993). Automatic, localizedin Vivo adjustment of all first-and second-order shim coils. Magn. Reson. Med. *29*, 804–811. 10.1002/mrm.1910290613.

99. Mekle, R., Mlynárik, V., Gambarota, G., Hergt, M., Krueger, G., and Gruetter, R. (2009). MR spectroscopy of the human brain with enhanced signal intensity at ultrashort echo times on a clinical platform at 3T and 7T. Magn. Reson. Med. *61*, 1279–1285. 10.1002/mrm.21961.

100. Xin, L., Schaller, B., Mlynarik, V., Lu, H., and Gruetter, R. (2013). Proton T_1 relaxation times of metabolites in human occipital white and gray matter at 7 T: Metabolites T_1 Relaxation Times in Human Brain at 7 T. Magn. Reson. Med. *69*, 931–936. 10.1002/mrm.24352.

101. Provencher, S.W. (1993). Estimation of metabolite concentrations from localizedin vivo proton NMR spectra. Magn. Reson. Med. *30*, 672–679. 10.1002/mrm.1910300604.

102. Brett, M., Anton, J.-L., Valabregue, R., and Poline, J.-B. (2002). Region of interest analysis using an SPM toolbox. Neuroimage *16*, S497.

103. Daunizeau, J., Adam, V., and Rigoux, L. (2014). VBA: A Probabilistic Treatment of Nonlinear Models for Neurobiological and Behavioural Data. PLoS Comput. Biol. *10*, e1003441. 10.1371/journal.pcbi.1003441.

104. Bicego, M., and Baldo, S. (2016). Properties of the Box–Cox transformation for pattern classification. Neurocomputing *218*, 390–400. 10.1016/j.neucom.2016.08.081.

105. Bergstra, J., Yamins, D., and Cox, D.D. (2013). Making a Science of Model Search: Hyperparameter Optimization in Hundreds of Dimensions for Vision Architectures.

106. Lundberg, S.M., Erion, G.G., and Lee, S.-I. (2019). Consistent Individualized Feature Attribution for Tree Ensembles. Preprint at arXiv.

Figures

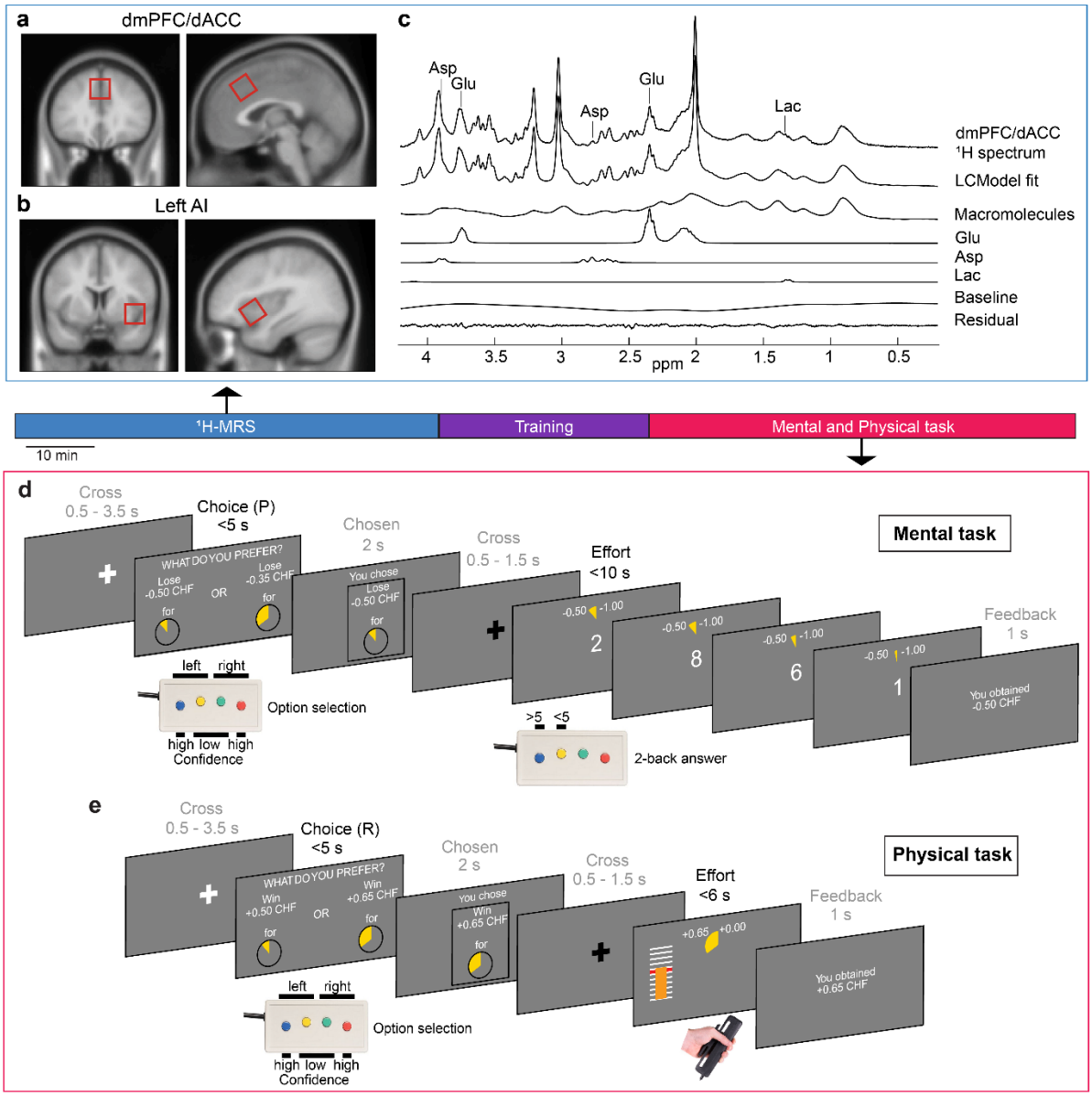

Fig. 1: Overview of experimental design. (**a-b**) Localization of dmPFC/dACC and AI voxels (20 x 20 x 20mm^3) targeted for ^{1}H-MRS acquisitions. The voxels are displayed in coronal and sagittal sections, overlaid on the MNI152 T1 average anatomical scan for reference. (**c**) Example of a ^{1}H-MR spectrum obtained from the dmPFC/dACC. The spectrum showcases the LGCModel spectral fit, macromolecular signals, baseline, residual fit, and individual metabolite fits for glutamate (Glu), aspartate (Asp), and lactate (Lac). (**d-e**) Effort-based decision-making tasks. Participants choose between options varying in effort and monetary incentive (reward or punishment) levels, with the potential for higher effort leading to greater rewards or avoiding larger punishments. Each trial started with a fixation cross, followed by a 5-seconds window where participants had to pick up the option that looked the more interesting for them based on their subjective preferences. There was always one option associated to a low effort and a low monetary incentive, while the other was associated to a larger monetary incentive but also to a higher effort. Physical and mental efforts were segregated into distinct blocks (2 for each type of effort), while rewards and punishment incentives were intermixed across trials within each block. After the choice was made, the chosen option was briefly displayed, followed by another fixation cross with a jitter to separate decision-making from the effort phase. (**d**) In the mental effort task, participants aimed to achieve a target number of correct responses within 10 seconds, determined by their prior calibration and the selected effort level. (**e**) In the physical effort task, participants had to maintain force above 55% of their

maximal force for a duration depending on the chosen effort level (between 0.5 and 4.5s). Each trial ended with performance feedback indicating how much money was earned (or lost respectively) in the current trial.

High Physical Effort
dmPFC/dACC
metabolites

Testing set:
r = 0.22, p = 0.22

Permutation test:
True RMSE = 23.00%
95th percentile
RMSE = 17.38 %

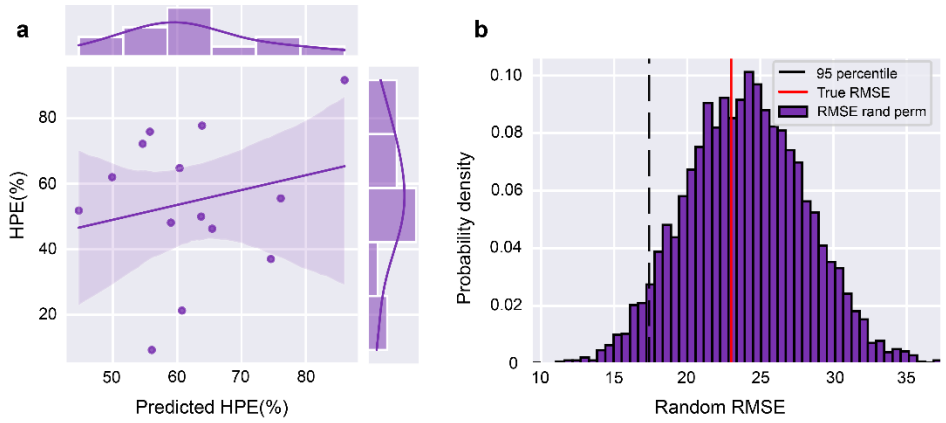

High Mental Effort
dmPFC/dACC
metabolites

Testing set:
r = 0.56, p = 0.02

Permutation test:
True RMSE = 12.37%
95th percentile
RMSE = 13.72 %

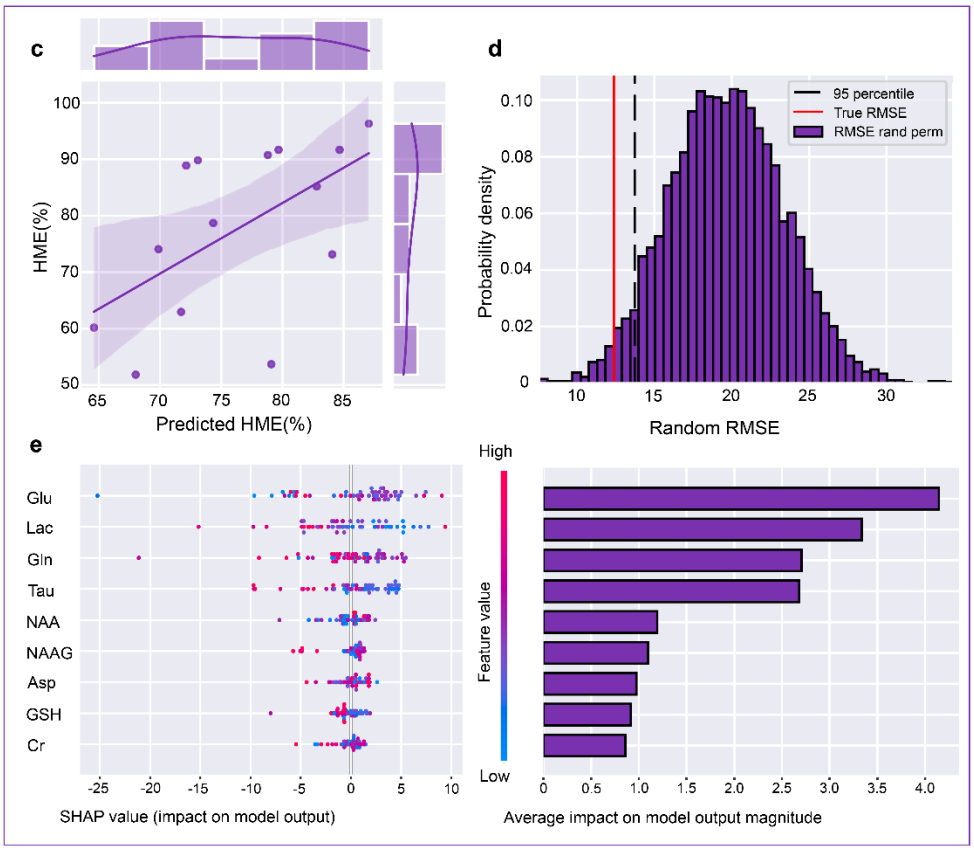

High Mental Effort
AI metabolites

Testing set:
r = -0.47, p = 0.06

Permutation test:
True RMSE = 23.28%
95th percentile
RMSE = 13.89 %

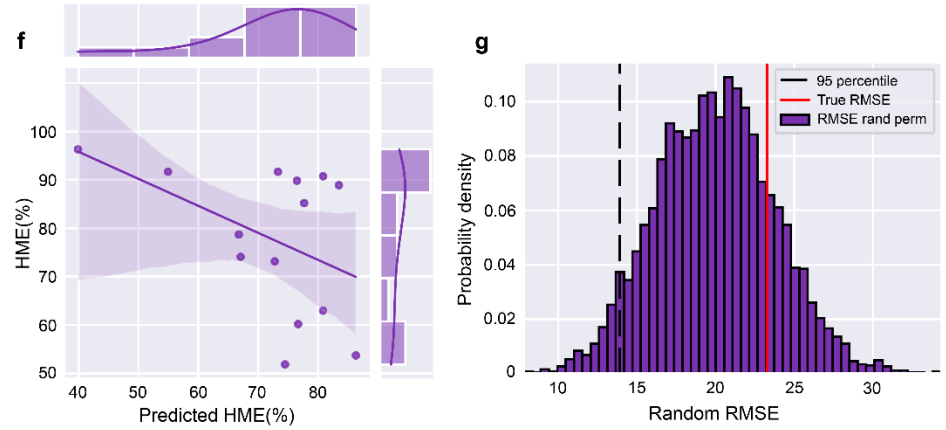

Fig. 2: Analysis of models' explanations for physical and mental effort choices based on metabolite concentrations in dmPFC/dACC and AI. (**a**) Analysis of high physical effort (HPE) explanations using dmPFC/dACC metabolite concentrations with an XGBoost model indicates a moderate correlation not reaching significance ($r = 0.22$, $p = 0.22$) for the test set. (**b**) Furthermore, a permutation test indicated lack of predictive robustness (95th percentile threshold = 17.38% vs. model RMSE = 23.00). (**c**), For high mental effort (HME) choices, our model showed a strong correlation ($r = 0.56$, $p = 0.02$), underscoring the model's efficacy in anticipating decision patterns based on dmPFC/dACC metabolite profiles. (**d**) Permutation test for HME predictions confirms model accuracy (95th percentile threshold = 13.72% vs. model RMSE = 12.37%). (**e**) Feature importance analysis via SHAP values for HME prediction identifies nine key metabolites: glutamate (Glu), lactate (Lac), glutamine (Gln), taurine (Tau), N-acetylaspartate (NAA), N-acetylaspartylglutamate (NAAG), aspartate (Asp), glutathione (GSH), and creatine (Cr). (**f**) A model trained on AI metabolites' predictive power for HME reveals a negative correlation between predicted and actual HME that does not reach statistical significance ($r = -0.47$, $p = 0.06$). (**g**), A permutation test further indicates a significant deviation in model performance for AI-based predictions (95th percentile threshold = 13.89% vs. model RMSE = 23.28%), highlighting a failure to predict HME choices based on AI metabolites.

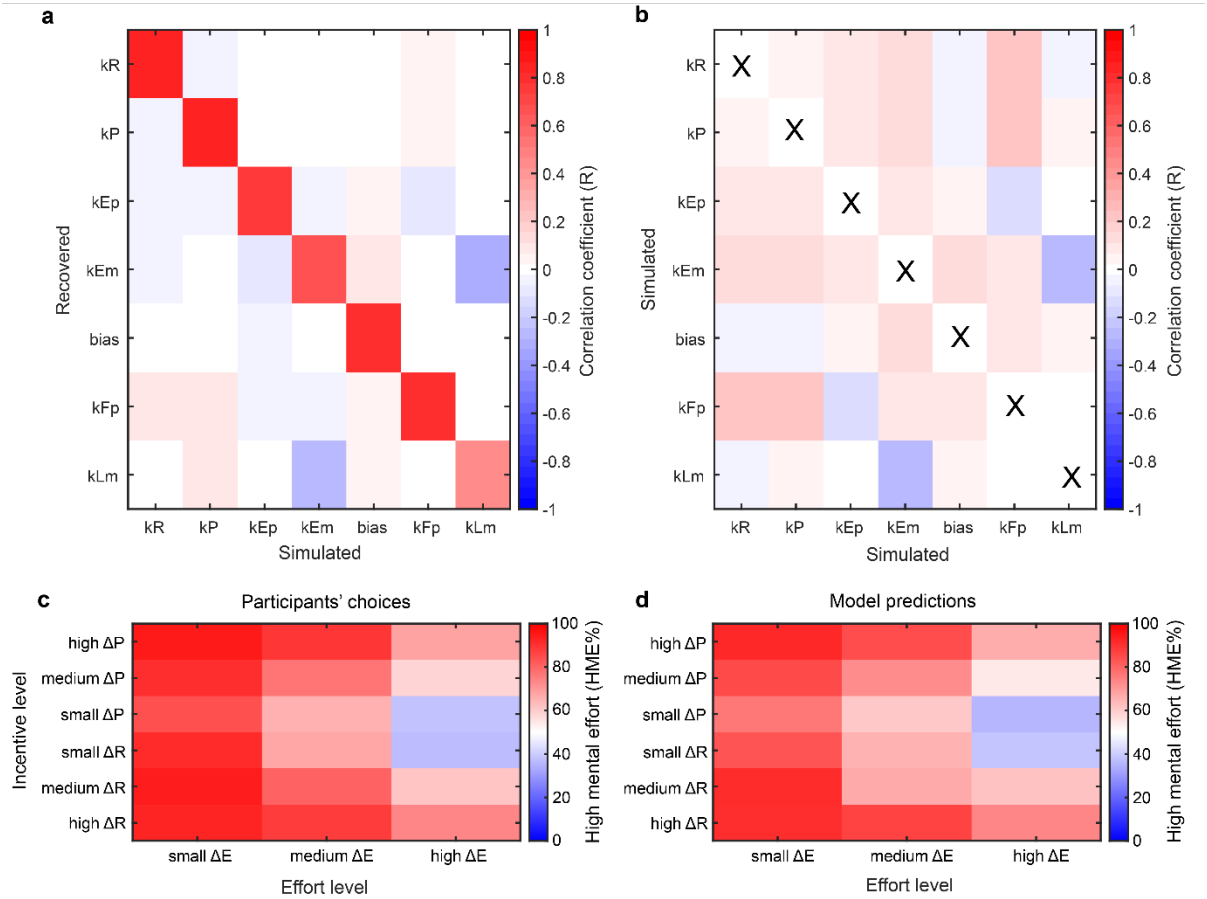

Fig. 3: Comprehensive analysis of model parameters. (**a**) Confusion matrix evaluating the model's parameter recovery capability, contrasting recovered parameters against their original (simulated) counterparts. The parameters correspond to the sensitivity for reward (kR), punishment (kP), physical effort (kEp), mental effort (kEm), a bias toward the high effort option (bias), physical fatigue (kFp) and mental learning (kLm). (**b**) Autocorrelation matrix derived from 30'000 simulations assessing the identifiability of all model parameters. (**c**) Heatmap representing the percentage of high mental effort (HME) choices in function of the difference between the high and the low effort option in terms of effort and incentive levels across participants. (**d**) Corresponding heatmap representing the percentage of high mental effort (HME) choices predicted by our computational model in function of the difference between the high and the low effort option in terms of effort and incentive levels.

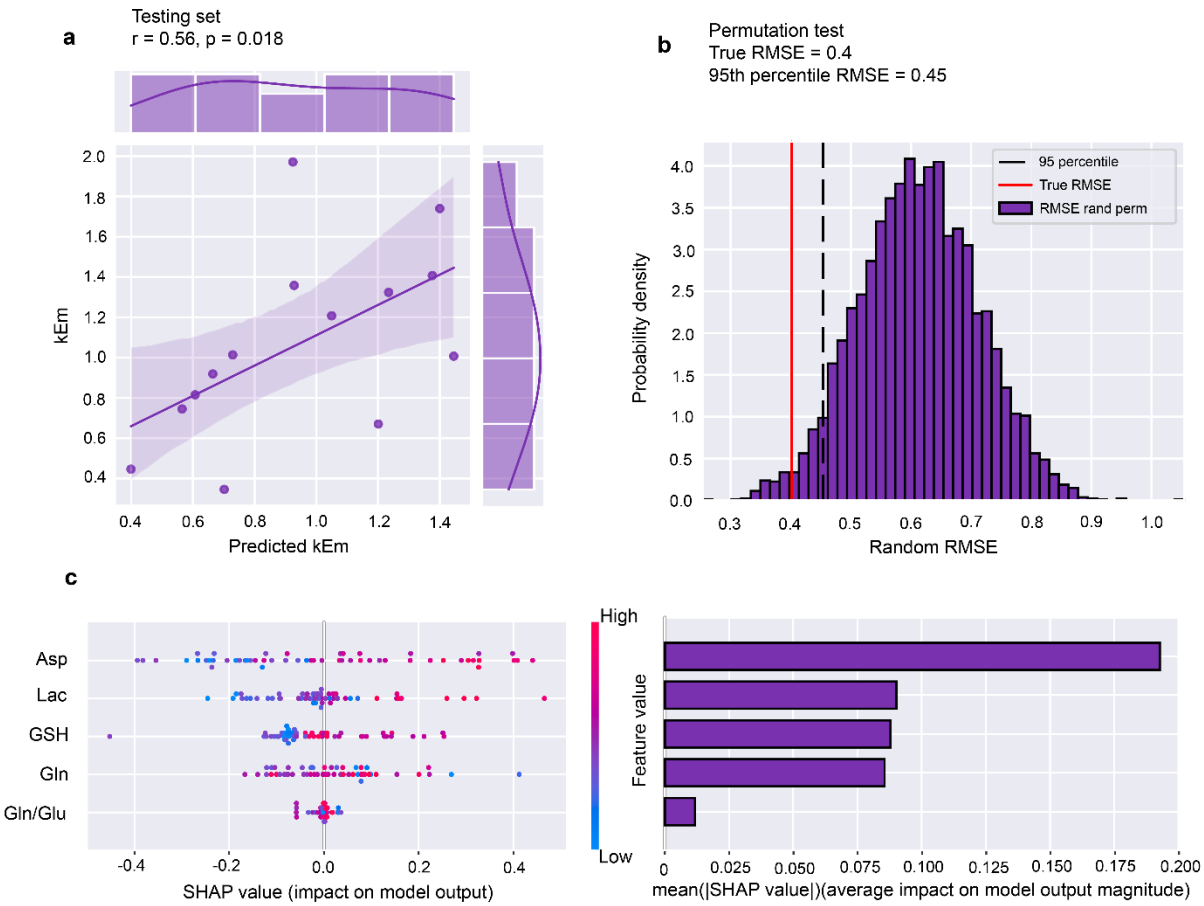

Fig. 4: Assessment of the model's explanatory power for mental effort sensitivity (kEm) using dmPFC/dACC metabolite concentrations. (**a**) A model based on dmPFC/dACC metabolites selected through an automated feature selection process shows a positive correlation (r = 0.56, p = 0.018) between predicted and observed values of kEm based on the XGBoost model's test set performance, highlighting the model's predictive accuracy. (**b**) Histogram of root mean square error (RMSE) from a permutation test involving random label permutation showing a clear validation of the model's robustness. The test, and the results show the model's RMSE (0.4) surpassing the 95th percentile of the permuted data (threshold RMSE = 0.45), confirming that the model's predictive success is not due to chance. (**c**) SHAP summary plot representing the impact of each feature on the model output for individual predictions. The analysis identifies five key metabolite parameters—Aspartate (Asp), Lactate (Lac), Glutathione (GSH), Glutamine (Gln), and the Glutamine/Glutamate (Gln/Glu) ratio—. Right panel: The horizontal dispersion of SHAP values per feature indicates the variability and influence of each on model predictions.

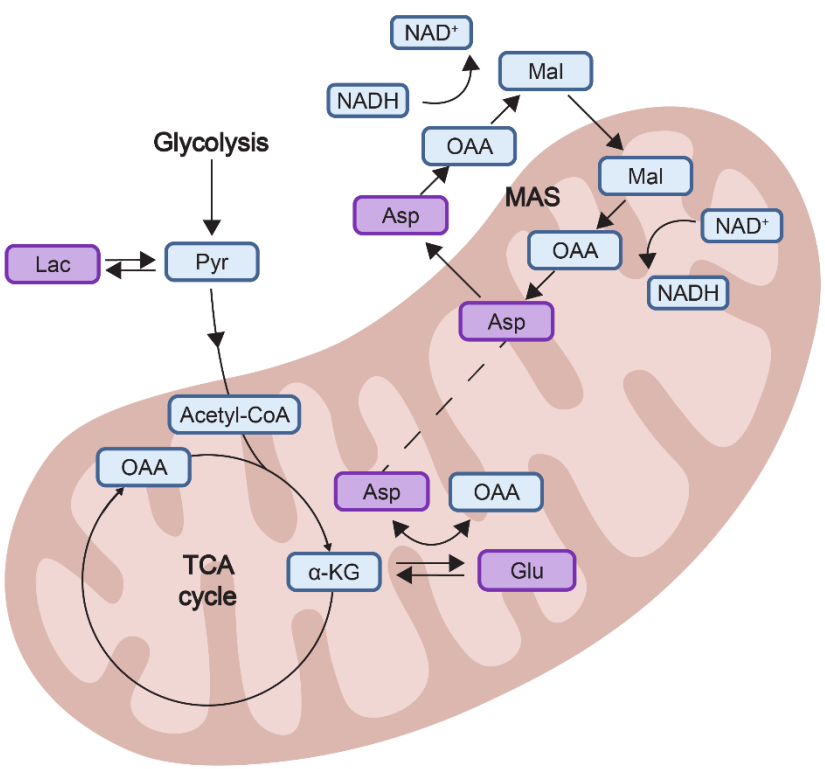

Fig. 5: Schematic representation of the identified metabolites within the tricarboxylic acid (TCA) cycle and the malate-aspartate shuttle (MAS) within mitochondria. The scheme depicts the interplay among key metabolites pertinent to neuronal energy metabolism. Highlighted in bold purple are the key metabolites related to mental effort motivation identified in this study: glutamate (Glu), aspartate (Asp), and lactate (Lac). The diagram traces the pathways of Asp and Glu within the TCA cycle and the role of Lac in glycolysis. Key intermediates include pyruvate (Pyr), alpha-ketoglutarate (α-KG), oxaloacetate (OAA), malate (Mal), and acetyl-CoA, along with the redox couple NAD+/NADH, integral to both the TCA cycle and MAS. This visual abstract underscores the metabolic fluxes that are hypothesized to underpin the cognitive processes.

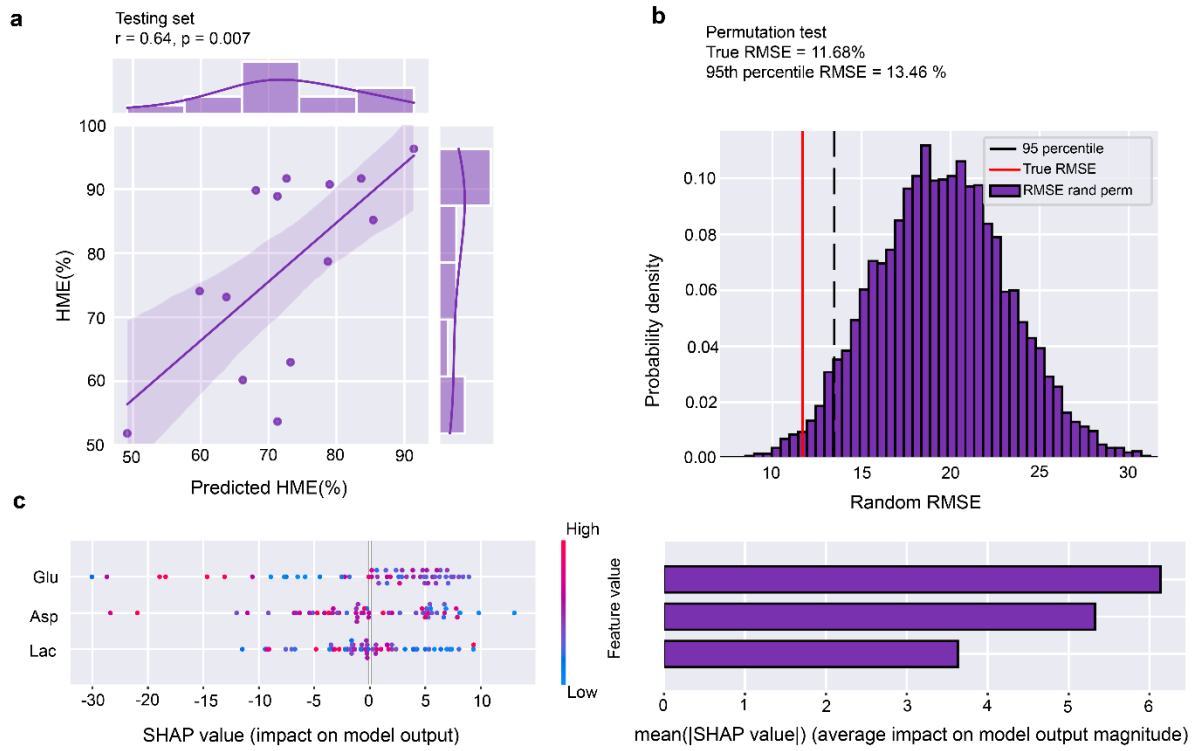

Fig. 6: Model for high mental effort (HME) choices using key metabolites from the dmPFC/dACC. (**a**) A strong positive correlation (r = 0.64, p = 0.007) between the XGBoost model's predicted probability of HME choices and the observed percentages within the test set, indicating robust predictive validity using the metabolites glutamate (Glu), aspartate (Asp), and lactate (Lac). (**b**) A permutation test that randomizes the labels and recalculates the RMSE to compare against the model's true performance indicates the model's predictive reliability, i.e., the true RMSE of the model (11.68%) is well below the 95th percentile of the permuted distribution (threshold RMSE = 13.46%), indicating that the model's predictions are not due to random chance. (**c**) SHAP value summary plot depicting the impact of each metabolite on the model's predictions for individual subjects. Right panel: The magnitude and distribution of the SHAP values for glutamate, aspartate, and lactate indicate their respective contributions to the model's decision-making process.

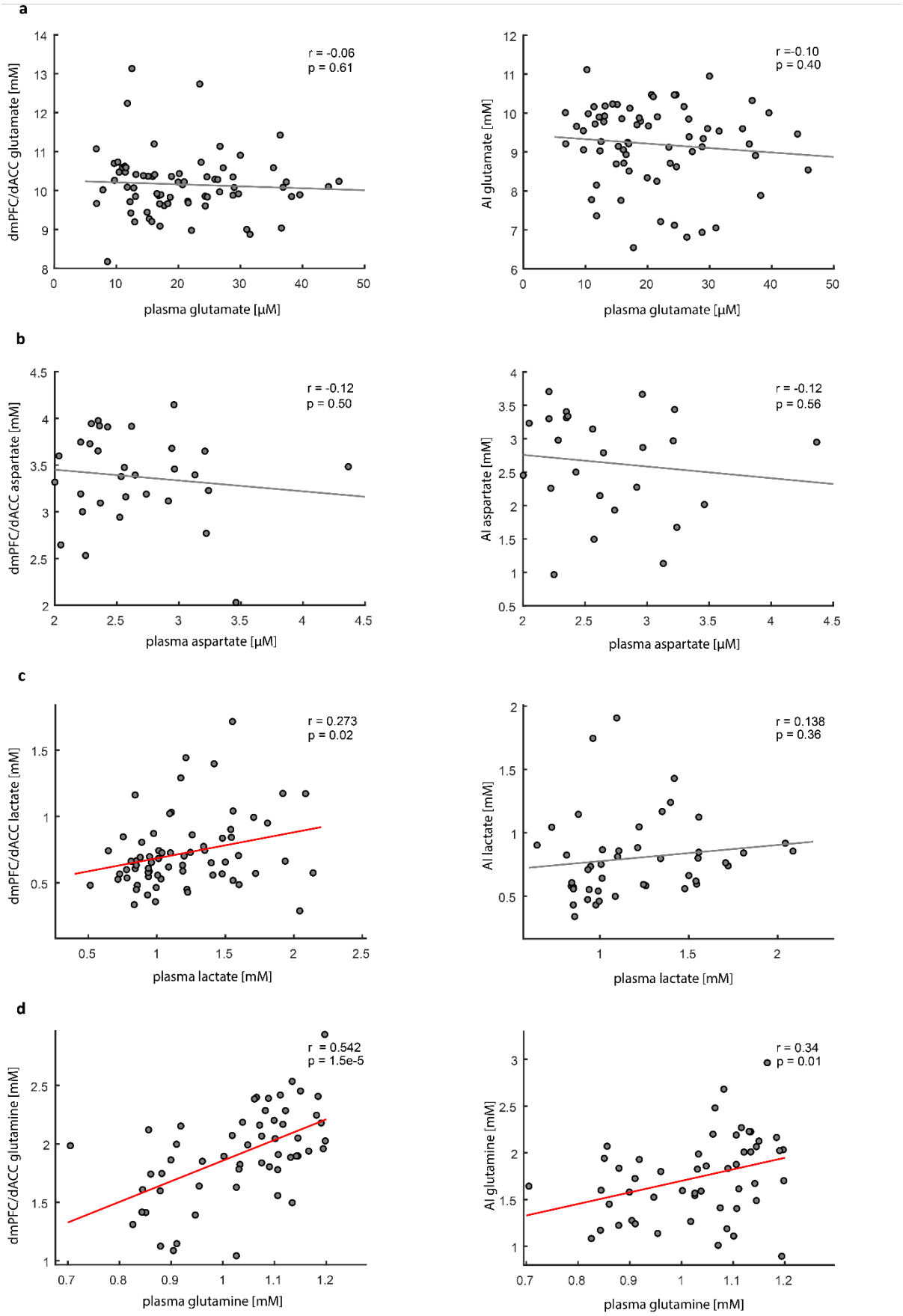
a
r = -0.06
p = 0.61
dmPFC/dACC glutamate [mM]
plasma glutamate [µM]
r =-0.10
p = 0.40
AI glutamate [mM]
plasma glutamate [µM]
b
r = -0.12
p = 0.50
dmPFC/dACC aspartate [mM]
plasma aspartate [µM]
r = -0.12
p = 0.56
AI aspartate [mM]
plasma aspartate [µM]
c
r = 0.273
p = 0.02
dmPFC/dACC lactate [mM]
plasma lactate [mM]
r = 0.138
p = 0.36
AI lactate [mM]
plasma lactate [mM]
d
r = 0.542
p = 1.5e-5
dmPFC/dACC glutamine [mM]
plasma glutamine [mM]
r = 0.34
p = 0.01
AI glutamine [mM]
plasma glutamine [mM]

Fig. 7: Cross-correlation of plasma and cerebral metabolite levels in the dmPFC/dACC and AI. (**a**) Glutamate shows no significant correlation between plasma and brain concentrations in either region (dmPFC/dACC: $r = -0.06$, $p = 0.61$; AI: $r = -0.10$, $p = 0.41$). (**b**) Aspartate levels also display no significant correlation in both regions (dmPFC/dACC: $r = 0.12$, $p = 0.51$; AI: $r = 0.12$, $p = 0.56$). (**c**) Lactate shows a weak but significant correlation in the dmPFC/dACC ($r = 0.27$, $p = 0.023$) but not in the AI ($r = 0.14$, $p = 0.36$). (**d**) Glutamine exhibits a moderate to strong correlation, significant in both regions (dmPFC/dACC: $r = 0.54$, $p < 0.001$; AI: $r = 0.34$, $p = 0.014$), suggesting a more pronounced relationship between plasma and brain levels compared to the other metabolites.